Doped Metal Oxide based Electron Transport Layer for Perovskite Solar Cells

By

Sana Mehmood

Reg No. 00000330715

Session 2020-2022

Supervised by

Dr. Nadia Shahzad

US-Pakistan Center for Advanced Studies in Energy (USPCAS-E)

National University of Sciences and Technology (NUST)

H-12, Islamabad 44000, Pakistan

July 2023

Doped Metal Oxide based Electron Transport Layer for Perovskite Solar Cells

By

Sana Mehmood

Reg No. 00000330715

Session 2020-2022

Supervised by

Dr. Nadia Shahzad

A Thesis Submitted to the US-Pakistan Center for Advanced Studies in Energy in partial fulfillment of the requirements for the degree of

MASTER of SCIENCE in

ENERGY SYSTEMS ENGINEERING

US-Pakistan Center for Advanced Studies in Energy (USPCAS-E)

National University of Sciences and Technology (NUST)

H-12, Islamabad 44000, Pakistan

July 2023

THESIS ACCEPTANCE CERTIFICATE

Certified that final copy of MS thesis written by **Ms. Sana Mehmood** (Registration No. 00000330715), of U.S.-Pakistan Center for Advanced Studies in Energy has been vetted by undersigned, found complete in all respects as per NUST Statues/Regulations, is within the similarity indices limit and is accepted as partial fulfillment for the award of MS degree. It is further certified that necessary amendments as pointed out by GEC members of the scholar have also been incorporated in the said thesis.

Signature: _____

Name of Supervisor: Dr. Nadia Shahzad

Date: 27/07/23

Signature (HoD): _____

Date: 27/7/2023

Signature (Dean/Principal): _____

Date: 27/7/2023

CERTIFICATE

This is to certify that work in this thesis has been carried out by **Ms. Sana Mehmood** and completed under my supervision in Solar Energy Research laboratory, US-Pakistan Center for Advanced Studies in Energy (USPCAS-E), National University of Sciences and Technology, H-12, Islamabad, Pakistan.

Supervisor:

Dr. Nadia Shahzad
USPCAS-E
NUST, Islamabad

GEC member 1:

Dr. Naseem Iqbal
USPCAS-E
NUST, Islamabad

GEC member 2:

Dr. Rabia Liaquat
USPCAS-E
NUST, Islamabad

GEC member 3:

Dr. M. Imran Shahzad
NS & TD
NCP, Islamabad

HOD-ESE/TEE/EPE:

Dr. Rabia Liaquat
USPCAS-E
NUST, Islamabad

Dean/Principal:

Dr. Adeel Waqas
USPCAS-E
NUST, Islamabad

Dedication

To the stars above, where memories align,
To a father whose love, transcends space and time.
In the celestial embrace, he guides my way,
His wisdom and care, in my heart, always.

To the mother, who in her arms, holds the world,
A beacon of strength, love unfurled.
With every step, her courage I've known,
A nurturer's touch, her love has shown.

To friends, who've walked beside me through strife,
Kindred spirits, who've colored my life.
A tapestry woven, with laughter and tears,
A testament of time, through the passing years.

To knowledge, that has lit my path to explore,
A journey to the depths, a quest for more.
In the halls of academia, my passion grew,
The pursuit of truth, to myself I've been true.

Acknowledgement

First and foremost, I express my deepest gratitude to **Almighty Allah**, the Creator of everything. And all respects for His **Prophet Muhammad** (PBUH, On Whom Be Allah's Blessings and Salutations). Without His divine blessings, this diligent and challenging task would have been impossible.

I wholeheartedly thank my supervisor, **Dr. Nadia Shahzad**, for her unwavering support, guidance, and invaluable experience in research. Her generosity in sharing her knowledge, providing freedom to explore research ideas, and fostering my research intuition has been instrumental in the completion of this work. I am eternally grateful for her kindness and patience throughout this journey.

I seize this opportunity to express my appreciation to all the Department faculty members for their assistance and encouragement. My special thanks extend to the lab engineers for their guidance during my work, as well as to my lab fellows for their continuous support during the long hours spent at the Solar Energy Research Lab.

Lastly, I convey my heartfelt regards to my GEC members for their steadfast support and guidance throughout this research project. I am also grateful to USPCAS-E for allowing me to use their state-of-the-art lab facilities. This thesis stands as a testament to the collective wisdom, dedication, and perseverance of all who have contributed to its completion.

Sana Mehmood

Abstract

Perovskite solar cells (PSCs) have attracted significant attention due to their higher efficiencies and lower fabrication costs. But for the better performance of PSCs, a high-quality electron transport layer (ETL) is crucial. Various ETLs have been employed and among them Tin (IV) oxide (SnO_2) has emerged as a promising candidate for electron selective layer in PSCs due to its superior optical and electrical characteristics. However, there is still improvement needed in terms of poor surface morphology and conductivities of SnO_2. When SnO_2 is used in conjunction with absorber layer in ambient conditions, stability, and charge carrier recombinations at SnO_2/perovskite interface remains a serious challenge as well. This study presents the doping of lanthanum (La III), a rare earth element, into SnO_2 ETLs to improve the quality and performance of the perovskite layer deposited on top of ETL in ambient condition. With the optimized 4% La (III) doping, SnO_2 ETLs become more crystalline with lower parasitic light absorption and surface morphology improves significantly. The improvement in morphology due to doping facilitates larger crystal growth of perovskite in ambient environment. Moreover, Photoluminescence reveals that with optimized level of doping, interfacial charge recombinations are significantly mitigated ensuring smooth injection of electrons into ETL because of superior perovskite film quality. The mixed-cation mixed-halide perovskite film deposited on 4% La-doped ETL show better resistance towards moisture ingress and will substantially contribute to develop long-life of planar PSCs.

Keywords: Electron transport layer, perovskite solar cells, ambient fabrication, elemental doping

Table of Contents

List of Figures

List of Tables

Publications

1. **Sana Mehmood**; Nadia Shahzad; Saad Nadeem; Muhammad Salik Qureshi; Abdul Sattar; Naseem Iqbal; Rabia Liaquat; Muhammad Imran Shahzad, **"Effect of lanthanum doped SnO_2 on the performance of mixed-cation mixed-halide perovskite for planar PSCs"**, *Thin Solid Films* (Submitted).

2. Saad Nadeem; Nadia Shahzad; **Sana Mehmood**; Muhammad Salik Qureshi; Abdul Sattar; Rabia Liaquat; Sehar Shakir; Muhammad Imran Shahzad, **"Solution-Processed Zn_2SnO_4 / ZTO Electron Transport Layers for Planar Perovskite Solar Cells"**, *Journal of Materials Science: Materials in Electronics* (Submitted).

3. Muhammad Salik Qureshi; Nadia Shahzad; Saad Nadeem; **Sana Mehmood**; Abdul Sattar; Sehar Shakir; Muhammad Imran Shahzad, **"Study of optical and electrical properties of SnO_2-MoS_2 electron transport layer for perovskite solar cell"** (In Submission Process).

4. Muniba Ayub; Ahad Hussain Javed; Nadia Shahzad; Zuhair S. Khan; Sehar Shakir; Faroha Liaqat; Ghulam Shabir; Faisal Abbas; **Sana Mehmood**; Muhammad Imran Shahzad, **"Comparative study of Ruthenium complexes and organic sensitizer in ZnO based Dye-sensitized solar cell",** *Energies* (In Submission Process).

List of Abbreviations

ETL	Electron Transport Layer
HTL	Hole Transport Layer
PSCs	Perovskite solar cell
J_{SC}	Short circuit current density
V_{OC}	Open circuit voltage
FF	Fill-factor
PCE	Power conversion efficiency
La	Lanthanum
FA	Formamidinium
CA	Contact Angle
MA	Methylammonium
FTO	Fluorine doped tin oxide
RT	Room temperature
TCO	Transparent conductive oxide
DMF	Dimethylformamide
DMSO	Dimethyl Sulfoxide
Ag	Silver
DSSCs	Dye sensitized solar cells
PCBM	Phenyl-C61-butyric acid methyl ester
Cu	Copper
PL	Photoluminescence
PSKT	Perovskite
Meso	Mesoporous
ITO	Indium tin oxide
Au	Gold

Chapter 01
Introduction

1.1 Introduction

The global urgency to transition towards clean and renewable energy sources has fueled extensive research in the solar energy domain [1] This push is driven by the increasing concerns about climate change, depleting fossil fuels, and the need to meet the ever-growing demand for energy. Among the numerous photovoltaic technologies studied, perovskite solar cells (PSCs) have captured the attention of researchers and the solar industry, owing to their exceptional properties [2].

Perovskite solar cells (PSCs) have seen a rapid growth in power conversion efficiency, ranging from 3.8% to 25.8%, and are becoming increasingly popular due to their high efficiency, ease of manufacturing, and affordability [1], [3]–[5]. Organic-inorganic halide perovskite materials have arisen as a research priority, leading to top-performing PSCs due to their remarkable optoelectronic features such as high absorption coefficients [6], high carrier mobility [7], and variable bandgaps [8]. The rapid development of these hybrid PSCs has sparked the solar industry's interest as a viable alternative to conventional photovoltaic systems [9]. Because of their great mechanical flexibility, low temperature produced lead halide perovskites also hold promise for extremely efficient, lightweight, and flexible solar systems [10]. While their conversion efficiencies are comparable to those of commercially available crystalline silicon solar cells, many critical limitations prevent perovskite materials from being widely adopted and commercialized [11]. Among these issues include the fundamental ionic properties [11] and delicate framework [12] [13] of perovskite materials, as well as considerable charge recombination between different contact layers [14].

To unlock the full potential of PSCs, a thorough understanding and optimization of ETL properties are necessary. This thesis aims to contribute to this endeavor by investigating the development and characterization of doped metal oxide based ETLs for PSCs. This research seeks to identify lanthanide doped ETL composition and strategies that can

further enhance the performance and stability of PSCs, paving the way for their large-scale deployment and commercialization.

1.2 Perovskite Solar Cells (PSCs)

1.2.1 Structure and Working Principle

Perovskite solar cells (PSCs) are a unique class of photovoltaic devices that utilize a perovskite material as the light-absorbing layer [15]. The general structure of a PSC consists of three primary layers: a perovskite absorber layer, a hole transport layer (HTL), and an electron transport layer [16]. These layers are carefully assembled to form a sandwich-like configuration that enables efficient charge separation and transport within the device. The perovskite absorber layer is the heart of the PSC, responsible for absorbing incident sunlight and generating excitons, which are bound electron-hole pairs. Perovskite materials exhibit exceptional light absorption properties, with high absorption coefficients [7] and tunable bandgaps, allowing them to harvest a broad range of the solar spectrum [6].

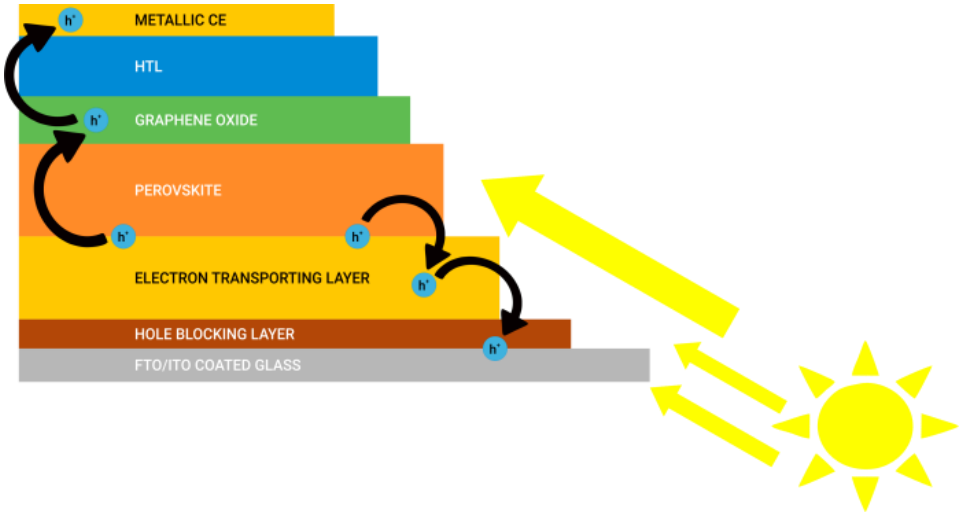

Figure 1.1. General working principle of PSCs [17]

Upon the absorption of light by the perovskite layer, excitons are generated within the material. These excitons then rapidly dissociate into free electrons and holes, primarily due to the strong electric field at the interfaces between the perovskite and the transport layers [18]. Efficient charge separation is crucial for minimizing recombination losses and

maximizing the overall efficiency of the solar cell [19]. Once the charges are separated, they need to be transported to their respective electrodes to create a flow of current through an external circuit. This is where the electron transport layer (ETL) and hole transport layer (HTL) come into play. The ETL selectively collects the free electrons generated in the perovskite layer and guides them towards the negative electrode (cathode), while the HTL performs a similar function for holes, directing them towards the positive electrode (anode) [16]. The selective nature of the ETL and HTL ensures minimal cross-recombination between the electrons and holes, allowing for efficient charge extraction and transport.

The synergistic operation of the perovskite absorber layer, ETL, and HTL is critical for the high performance of PSCs. Their respective properties, such as energy levels, conductivity, and interface quality, must be carefully optimized to ensure maximum charge separation, collection, and transport, ultimately leading to a high-power conversion efficiency in the resulting solar cell [20].

1.2.2 Advantages and Challenges

Perovskite solar cells (PSCs) are an emerging technology that has garnered significant attention in the renewable energy sector due to their impressive qualities. They exhibit high power conversion efficiency [6], which means that they can effectively convert sunlight into usable electricity with minimal losses. This efficiency is comparable to, and in some cases even surpasses, that of traditional silicon-based solar cells, making PSCs a highly promising alternative for solar energy generation.

Another major advantage of PSCs is their low production cost [21]. Unlike silicon solar cells, which require expensive and energy-intensive manufacturing processes, PSCs can be fabricated using solution-based techniques. This involves dissolving the perovskite materials in a solvent and then depositing the resulting solution onto a substrate using methods such as spin-coating or inkjet printing. The ease and affordability of these processes significantly reduces the overall cost of producing PSCs, making them an attractive option for widespread deployment. Furthermore, the solution processability of PSCs allows for the possibility of producing lightweight, flexible, and semi-transparent

solar cells [22]. These attributes open up a wide range of potential applications, such as integration into building materials, portable electronics, etc.

Despite these advantages, there are a few key challenges that must be addressed before PSCs can be commercialized on a large scale. One of the primary concerns is the long-term stability of the devices [11]. PSCs are known to degrade over time, particularly when exposed to moisture, oxygen, and temperature fluctuations. This degradation can significantly reduce their efficiency and shorten their operational lifespan, making them less competitive with established solar cell technologies. Another crucial issue is the toxicity of lead-based perovskites, which are commonly used in PSCs due to their excellent photovoltaic properties [23]. The presence of lead poses both environmental and health risks, raising concerns about the safety and sustainability of using these materials in solar cells. To mitigate these risks, researchers are exploring alternative materials, such as tin or bismuth-based perovskites, that can provide comparable performance without toxic elements.

Perovskite solar cells have the potential to revolutionize the solar energy industry due to their high efficiency, low production cost, and solution processability. However, overcoming the challenges of long-term stability and lead toxicity is essential for the successful commercialization and widespread adoption of this promising technology.

1.3 Electron Transport Layers in PSCs

1.3.1 Role and Importance

Electron transport layers serve a crucial function within perovskite solar cells (PSCs) and directly influence their performance, stability, and efficiency [16]. ETLs are responsible for several key processes in PSCs, which are discussed in detail below:

1.3.1.1 Efficient Charge Extraction

The primary role of ETLs is to selectively collect and extract electrons generated in the perovskite layer upon light absorption [19]. By providing an energetically favorable pathway for electrons to flow, ETLs ensure that the charges are efficiently separated,

reducing the probability of recombination [24] with holes in the perovskite layer or at the perovskite/HTL interface.

1.3.1.2 Charge Transport

After extracting the electrons from the perovskite layer, ETLs are responsible for transporting them towards the cathode. High electron mobility and appropriate energy level alignment between the ETL and the perovskite layer are crucial factors in enabling rapid and efficient charge transport, minimizing resistive losses, and increasing overall device performance [25].

1.3.1.3 Recombination Suppression

ETLs play a vital role in suppressing unwanted charge recombination events, which can significantly reduce the solar cell's efficiency. By selectively extracting and transporting electrons, ETLs help maintain charge separation and prevent recombination at the interfaces and within the transport layers [26].

1.3.1.4 Device Stability

ETLs can contribute to the long-term stability of PSCs by acting as a barrier against moisture, oxygen, and other environmental factors that can degrade the perovskite layer [27]. In addition, the chemical compatibility between the ETL and the perovskite layer can influence the device's overall stability, as certain ETL materials might react with the perovskite or cause degradation.

1.3.1.5 Interface Quality

The quality of the interface between the ETL and the perovskite layer is crucial for efficient charge extraction and transport. Defects, impurities, or roughness at the interface can lead to charge trapping or recombination, negatively impacting the device performance [28]. ETL materials and deposition techniques should be carefully chosen to ensure high-quality interfaces.

The choice of ETL material and optimization of its properties are critical factors in determining the overall efficiency, stability, and performance of PSCs. Consequently, the development and investigation of novel ETL materials, doping strategies, and fabrication

methods are essential for advancing PSC technology and bringing it closer to commercialization.

1.3.2 Commonly Used ETL Materials

Electron transport layers (ETLs) play a crucial role in perovskite solar cells (PSCs) by facilitating efficient charge extraction and transport. Among the various ETL materials, compact and mesoporous metal oxides, such as TiO_2, SnO_2, and ZnO, are commonly employed due to their desirable characteristics. In this section, we discuss the advantages and limitations of each ETL material.

1.3.2.1 Titanium Dioxide (TiO_2)

Titanium dioxide (TiO_2) is commonly recognized as an n-type semiconductor, with conductivity resulting from oxygen vacancies created during the production process. This material boasts several advantages, such as a sizable band gap (3.0-3.2 eV) [29], compatibility with the energy band of the perovskite layer, and ease of production. Additionally, TiO_2 exhibits strong thermal and chemical stability while offering cost-effective manufacturing [29].

However, to achieve crystallinity and high carrier mobility in TiO_2, it must undergo high-temperature sintering (>450 °C), which complicates fabrication techniques and limits the progress of flexible devices [30]. Due to the slow carrier migration rate and deep level defects in TiO_2, electrons originating from the perovskite layer face difficulties in efficient transportation, leading to suboptimal device performance. Furthermore, TiO_2 experiences low photon absorption [31].

1.3.2.2 Tin Dioxide (SnO_2)

Tin (IV) oxide (SnO_2 has gained attention as an effective electron transport layer (ETL) due to its unique attributes, including high optical transparency (>85%) in the visible spectrum [32], affordability, low cost [32], superior electron mobility ($24 cm^2/V.s$) [33], photostability, low temperature processability, and appropriate band energy alignment [34] relative to the HOMO position of standard perovskites. In comparison to TiO_2, SnO_2 not only exhibits greater electron charge carrier mobility but also a broader optical band edge

(3.6-4.1 eV) [35], [36] is advantageous for the development of high-performance perovskite solar cells (PSCs).

However, imperfections within the SnO_2 crystal structure, such as tin interstitials and oxygen voids [37], typically hinder the enhancement of the Jsc in PSCs. SnO_2 exhibits spontaneous aggregation, leading to pinholes or island-like structures, which contribute to poor thin film morphology [38].

1.3.2.3 Zinc Oxide (ZnO)

Zinc oxide (ZnO), a broad bandgap material with exceptional electronic properties, is regarded as an ideal electron transport layer (ETL) material for perovskite solar cells (PSCs). ZnO holds a notable advantage over the commonly used titanium dioxide (TiO_2) in terms of easily fabricating diverse nanostructures at low temperatures through solution-based processes, while also enabling customization of their outstanding electrical and optical traits by adjusting their morphology and composition [39], [40].

However, ZnO typical conduction band minimum (CBM) of 4.4 eV is significantly lower than that of perovskite. This unfavorable band alignment, where the ETL's CBM is considerably lower than perovskite's, leads to increased interface recombination and consequently degrades the open-circuit voltage (V_{oc}) [39], [40].

TiO_2, SnO_2, and ZnO are commonly used ETL materials in PSCs due to their favorable properties, such as high electron mobility, suitable energy levels, and chemical stability. However, each material also has its limitations, which must be carefully considered and addressed to optimize the performance and stability of PSCs. Further research and development of novel ETL materials and strategies are essential for advancing PSC technology and enabling its widespread commercialization.

1.4 Doped Metal Oxide ETLs

Doping is a widely employed strategy in materials science that involves the deliberate introduction of impurities, also known as dopants, into a host material. The primary aim of doping is to modify and optimize the host material's electrical, optical, or structural properties, leading to improved performance in specific applications. Employing doping

techniques has proven to be an effective method for refining the electronic and interfacial properties of ETL by inducing suitable alignment of energy levels [41]. As a result, this optimization process minimizes charge accumulation and recombination at the interface while simultaneously boosting electron extraction and hysteresis in PSCs [42].

1.4.1. Advantages of Doped Metal Oxide ETLs

Doped metal oxide electron transport layers (ETLs) have garnered significant interest in perovskite solar cells (PSCs) research due to the numerous advantages they offer in terms of device performance and stability. By carefully selecting dopants and optimizing the doping process, it is possible to achieve significant improvements in PSC efficiency and long-term stability. In this section, we discuss the advantages of doped metal oxide ETLs in detail.

1.4.1.1 Improved Electron Mobility

Doping can increase the electron mobility of metal oxide ETLs by introducing additional free carriers (electrons) into the material. Higher electron mobility allows for more efficient charge extraction and transport, reducing resistive losses and improving the overall device performance. This is particularly beneficial for PSCs, as efficient charge transport is crucial for achieving high power conversion efficiencies.

1.4.1.2 Reduced Charge Recombination

Doped metal oxide ETLs can help suppress charge recombination by reducing the density of trap states and defects in the material. By passivating or eliminating these recombination centers, doped ETLs can maintain better charge separation and enhance the overall device efficiency. In addition, certain dopants can also modify the energy level alignment between the ETL and the perovskite layer, further reducing the likelihood of charge recombination at the interface.

1.4.1.3 Enhanced Energy Level Alignment

Optimal energy level alignment between the ETL and the perovskite layer is essential for efficient charge extraction and transport. Doping can modify the energy levels of metal oxide ETLs, allowing for better alignment with the perovskite layer and minimizing

recombination losses. This is particularly important for emerging perovskite materials with different bandgaps or energy level requirements, as conventional undoped ETLs may not provide the best energy level alignment for these systems.

1.4.1.4 Better Interface Quality

Doping can improve the interface quality between the ETL and the perovskite layer, which is crucial for efficient charge extraction and transport. By reducing defects, impurities, or roughness at the interface, doped metal oxide ETLs can minimize charge trapping or recombination and enhance device performance. In some cases, dopants can also promote better adhesion or compatibility between the ETL and the perovskite layer, further contributing to improved interface quality.

1.4.1.5 Enhanced Stability

Doped metal oxide ETLs can contribute to the long-term stability of PSCs by acting as a barrier against environmental factors such as moisture, oxygen, and UV radiation. The incorporation of dopants can modify the material's electronic and structural properties, leading to improved resistance against degradation mechanisms that can affect the perovskite layer. This is particularly important for the commercialization of PSCs, as long-term stability is a critical requirement for practical applications.

1.5 Problem Statement

Currently, SnO_2 is a widely used and researched ETL in perovskite solar cells. However, there are still some deficiencies in terms of carrier mobility, surface defects and degradation due to recombination which leads us to look out for other alternatives and test their compatibility with perovskite absorber layer.

1.6 Proposal

Elemental doping has evolved as a promising strategy to modulate the electronic and surface properties of SnO_2. La (III), being a rare earth metal, possesses unfilled 4f electronic shell, which gives La (III) its exceptional optoelectronic characteristics. When Lanthanide (La) is integrated into ETL, it can influence ETL’s electrical, optical, and stability aspects.

1.7 Research Objectives

- Fabrication of doped metal oxide-based electron transport layer for perovskite solar cells.
- Optical and electrical properties, characterization, and morphological studies of the doped metal-oxide based ETLs.
- Optimization and suitability of the prepared ETL for perovskite solar cells.

Summary

This chapter provides an overview of perovskite solar cells (PSCs) and their electron transport layers (ETLs). The chapter begins with an introduction to the topic and then delves into the specifics of PSCs, including their structure and working principle, as well as their advantages and challenges. The role and importance of ETLs in PSCs are then discussed, along with the commonly used materials for ETLs. The chapter also explores doped metal oxide ETLs and the advantages they offer. Thin film deposition techniques are then covered in detail, including chemical bath deposition, spin coating, physical vapor deposition, atomic layer deposition (ALD), and the sol-gel process. The chapter concludes with a problem statement, proposal, and research objectives. Overall, the chapter provides a comprehensive overview of the important concepts related to PSCs and ETLs.

References

[1] Enhanced electron extraction using SnO2 for high-efficiency planar-structure HC(NH2)2PbI3-based perovskite solar cells. Nature Energy, 2(1), 16177 | 10.1038/nenergy.2016.177." https://sci-hub.se/10.1038/nenergy.2016.177 (accessed Apr. 10, 2023).

[2] A. Paul, B. Sarkar, S. Paul, Sk. A. Moyez, H. S. Jung, and S. Roy, "From 3.8% to over 23.8% Power Conversion Efficiency: Commercial Perovskite Solar Cells, Significant Manufacturing Techniques, and Future Prospects," *Reference Module in Materials Science and Materials Engineering*, pp. 418–433, Jan. 2023, doi: 10.1016/B978-0-12-819728-8.00044-9.

[3] Improved High-Efficiency Perovskite Planar Heterojunction Solar Cells via Incorporation of a Polyelectrolyte Interlayer. Chemistry of Materials, 26(18), 5190–5193 | 10.1021/cm502864s." https://sci-hub.se/https://doi.org/10.1021/cm502864s (accessed Apr. 10, 2023).

[4] "Sci-Hub | Solvent annealing of PbI2for the high-quality crystallization of perovskite films for solar cells with efficiencies exceeding 18%. Nanoscale, 8(47), 19654–19661 | 10.1039/c6nr07076k." https://sci-hub.se/https://doi.org/10.1039/C6NR07076K (accessed Apr. 10, 2023).

[5] H. V. Quy and C. W. Bark, "Ni-Doped SnO2as an Electron Transport Layer by a Low-Temperature Process in Planar Perovskite Solar Cells," *ACS Omega*, vol. 7, no. 26, pp. 22256–22262, Jul. 2022, doi: 10.1021/acsomega.2c00965.

[6] Organometal Halide Perovskites as Visible-Light Sensitizers for Photovoltaic Cells. Journal of the American Chemical Society, 131(17), 6050–6051 | 10.1021/ja809598r." https://sci-hub.se/https://doi.org/10.1021/ja809598r (accessed Apr. 10, 2023).

[7] G. W. P. Adhyaksa, L. W. Veldhuizen, Y. Kuang, S. Brittman, R. E. I. Schropp, and E. C. Garnett, "Carrier Diffusion Lengths in Hybrid Perovskites: Processing, Composition, Aging, and Surface Passivation Effects," *Chemistry of Materials*, vol.

28, no. 15, pp. 5259–5263, Aug. 2016, doi: 10.1021/ACS.CHEMMATER.6B00466/SUPPL_FILE/CM6B00466_SI_001.PDF.

[8] T. C. J. Yang, P. Fiala, Q. Jeangros, and C. Ballif, "High-Bandgap Perovskite Materials for Multijunction Solar Cells," *Joule*, vol. 2, no. 8, pp. 1421–1436, Aug. 2018, doi: 10.1016/J.JOULE.2018.05.008.

[9] M. Park, J. Y. Kim, H. J. Son, C. H. Lee, S. S. Jang, and M. J. Ko, "Low-temperature solution-processed Li-doped SnO2 as an effective electron transporting layer for high-performance flexible and wearable perovskite solar cells," *Nano Energy*, vol. 26, pp. 208–215, Aug. 2016, doi: 10.1016/j.nanoen.2016.04.060.

[10] D. Yang, R. Yang, S. Priya, and S. (Frank) Liu, "Recent Advances in Flexible Perovskite Solar Cells: Fabrication and Applications," *Angewandte Chemie International Edition*, vol. 58, no. 14, pp. 4466–4483, Mar. 2019, doi: 10.1002/ANIE.201809781.

[11] T. A. Chowdhury, M. A. Bin Zafar, M. Sajjad-Ul Islam, M. Shahinuzzaman, M. A. Islam, and M. U. Khandaker, "Stability of perovskite solar cells: issues and prospects," *RSC Adv*, vol. 13, no. 3, pp. 1787–1810, Jan. 2023, doi: 10.1039/D2RA05903G.

[12] B. Chen, P. N. Rudd, S. Yang, Y. Yuan, and J. Huang, "Imperfections and their passivation in halide perovskite solar cells," *Chem Soc Rev*, vol. 48, no. 14, pp. 3842–3867, Jul. 2019, doi: 10.1039/C8CS00853A.

[13] J. P. Correa-Baena *et al.*, "Promises and challenges of perovskite solar cells," *Science (1979)*, vol. 358, no. 6364, pp. 739–744, Nov. 2017, doi: 10.1126/SCIENCE.AAM6323/SUPPL_FILE/AAM6323_CORREA-BAENA_SM.PDF.

[14] H. Zhou *et al.*, "Interface engineering of highly efficient perovskite solar cells," *Science (1979)*, vol. 345, no. 6196, pp. 542–546, Aug. 2014, doi: 10.1126/SCIENCE.1254050/SUPPL_FILE/ZHOU.SM.PDF.

[15] R. K. Battula, E. Ramasamy, P. Bhyrappa, C. Sudakar, and G. Veerappan, "Oxide free materials for perovskite solar cells," *Oxide Free Nanomaterials for Energy Storage and Conversion Applications*, pp. 287–306, Jan. 2022, doi: 10.1016/B978-0-12-823936-0.00001-2.

[16] P. Roy, N. K. Sinha, and A. Khare, "Progress in efficiency and stability of hybrid perovskite photovoltaic devices in high reactive environments," *Hybrid Perovskite Composite Materials: Design to Applications*, pp. 239–257, Jan. 2021, doi: 10.1016/B978-0-12-819977-0.00011-1.

[17] P. Ghosh, S. Sundaram, T. P. Nixon, and S. Krishnamurthy, "Influence of Nanostructures in Perovskite Solar Cells," *Encyclopedia of Smart Materials*, pp. 646–660, Jan. 2021, doi: 10.1016/B978-0-12-815732-9.00054-1.

[18] "(17) (PDF) Development of new inorganic p-type materials for perovskite solar cells." https://www.researchgate.net/publication/341654182_Development_of_new_inorganic_p-type_materials_for_perovskite_solar_cells (accessed Apr. 29, 2023).

[19] L. Huang and Z. Ge, "Simple, Robust, and Going More Efficient: Recent Advance on Electron Transport Layer-Free Perovskite Solar Cells," *Adv Energy Mater*, vol. 9, no. 24, p. 1900248, Jun. 2019, doi: 10.1002/AENM.201900248.

[20] F. Baig, Y. H. Khattak, B. Marí, S. Beg, S. R. Gillani, and A. Ahmed, "Mitigation of interface recombination by careful selection of ETL for efficiency enhancement of MASnI3 solar cell," *Optik (Stuttg)*, vol. 170, pp. 463–474, Oct. 2018, doi: 10.1016/J.IJLEO.2018.05.135.

[21] M. Cai *et al.*, "Cost-Performance Analysis of Perovskite Solar Modules," *Advanced Science*, vol. 4, no. 1, p. 1600269, Jan. 2017, doi: 10.1002/ADVS.201600269.

[22] D. Yang, R. Yang, S. Priya, and S. (Frank) Liu, "Recent Advances in Flexible Perovskite Solar Cells: Fabrication and Applications," *Angewandte Chemie - International Edition*, vol. 58, no. 14, pp. 4466–4483, Mar. 2019, doi: 10.1002/ANIE.201809781.

[23] M. Ren, X. Qian, Y. Chen, T. Wang, and Y. Zhao, "Potential lead toxicity and leakage issues on lead halide perovskite photovoltaics," *J Hazard Mater*, vol. 426, p. 127848, Mar. 2022, doi: 10.1016/J.JHAZMAT.2021.127848.

[24] W. Q. Wu, J. F. Liao, J. X. Zhong, Y. F. Xu, L. Wang, and J. Huang, "Suppressing Interfacial Charge Recombination in Electron-Transport-Layer-Free Perovskite Solar Cells to Give an Efficiency Exceeding 21 %," *Angewandte Chemie International Edition*, vol. 59, no. 47, pp. 20980–20987, Nov. 2020, doi: 10.1002/ANIE.202005680.

[25] Q. Guo *et al.*, "Effect of Energy Alignment, Electron Mobility, and Film Morphology of Perylene Diimide Based Polymers as Electron Transport Layer on the Performance of Perovskite Solar Cells," *ACS Appl Mater Interfaces*, vol. 9, no. 12, pp. 10983–10991, Mar. 2017, doi: 10.1021/ACSAMI.7B00902.

[26] J. Han *et al.*, "Efficient promotion of charge separation and suppression of charge recombination by blending PCBM and its dimer as electron transport layer in inverted perovskite solar cells," *RSC Adv*, vol. 6, no. 113, pp. 112512–112519, Nov. 2016, doi: 10.1039/C6RA22023A.

[27] L. Qian, Y. Zheng, J. Xue, and P. H. Holloway, "Stable and efficient quantum-dot light-emitting diodes based on solution-processed multilayer structures," *Nature Photonics 2011 5:9*, vol. 5, no. 9, pp. 543–548, Aug. 2011, doi: 10.1038/nphoton.2011.171.

[28] S. Sonmezoglu and S. Akin, "Suppression of the interface-dependent nonradiative recombination by using 2-methylbenzimidazole as interlayer for highly efficient and stable perovskite solar cells," *Nano Energy*, vol. 76, p. 105127, Oct. 2020, doi: 10.1016/J.NANOEN.2020.105127.

[29] R. Teimouri *et al.*, "Synthesizing Li doped TiO2 electron transport layers for highly efficient planar perovskite solar cell," *Superlattices Microstruct*, vol. 145, Sep. 2020, doi: 10.1016/j.spmi.2020.106627.

[30] H. Wang *et al.*, “W-doped TiO2 as electron transport layer for high performance solution-processed perovskite solar cells,” *Appl Surf Sci*, vol. 563, Oct. 2021, doi: 10.1016/j.apsusc.2021.150298.

[31] A. I. Rafieh, P. Ekanayake, A. L. Tan, and C. M. Lim, “Effects of ionic radii of co-dopants (Mg, Ca, Al and La) in TiO2 on performance of dye-sensitized solar cells,” *Solar Energy*, vol. 141, pp. 249–255, Jan. 2017, doi: 10.1016/j.solener.2016.11.052.

[32] X. Zhou *et al.*, “Solution-processed Cu-doped SnO2 as an effective electron transporting layer for High-Performance planar perovskite solar cells,” *Appl Surf Sci*, vol. 584, May 2022, doi: 10.1016/j.apsusc.2022.152651.

[33] A. F. Khan, M. Mehmood, M. Aslam, and M. Ashraf, “Characteristics of electron beam evaporated nanocrystalline SnO2 thin films annealed in air,” *Appl Surf Sci*, vol. 256, no. 7, pp. 2252–2258, Jan. 2010, doi: 10.1016/J.APSUSC.2009.10.047.

[34] J. Bahadur, A. H. Ghahremani, B. Martin, T. Druffel, M. K. Sunkara, and K. Pal, “Solution processed Mo doped SnO2 as an effective ETL in the fabrication of low temperature planer perovskite solar cell under ambient conditions,” *Org Electron*, vol. 67, pp. 159–167, Apr. 2019, doi: 10.1016/J.ORGEL.2019.01.027.

[35] N. Chiodini, A. Paleari, … D. D.-A. physics, and undefined 2002, “nanocrystals in A wide-band-gap quantum-dot system,” *aip.scitation.org*, vol. 81, no. 9, p. 1702, Aug. 2002, doi: 10.1063/1.1503154.

[36] L. Shi and H. Lin, “Preparation of band gap tunable SnO2 nanotubes and their ethanol sensing properties,” *Langmuir*, vol. 27, no. 7, pp. 3977–3981, Apr. 2011, doi: 10.1021/LA104529H/ASSET/IMAGES/MEDIUM/LA-2010-04529H_0004.GIF.

[37] R. Xue *et al.*, “Architecturing Lattice-Matched Bismuthene-SnO2Heterojunction for Effective Perovskite Solar Cells,” *ACS Sustain Chem Eng*, vol. 8, no. 29, pp. 10714–10725, Jul. 2020, doi: 10.1021/ACSSUSCHEMENG.0C01794.

[38] Z. Xu *et al.*, “La-doped SnO2 as ETL for efficient planar-structure hybrid perovskite solar cells,” *Org Electron*, vol. 73, pp. 62–68, Oct. 2019, doi: 10.1016/j.orgel.2019.03.053.

[39] H. Wang *et al.*, “NH4Cl-Modified ZnO for High-Performance CsPbIBr2 Perovskite Solar Cells via Low-Temperature Process,” *Solar RRL*, vol. 4, no. 1, p. 1900363, Jan. 2020, doi: 10.1002/SOLR.201900363.

[40] Y. Z. Zheng *et al.*, “Iodine-doped ZnO nanopillar arrays for perovskite solar cells with high efficiency up to 18.24%,” *J Mater Chem A Mater*, vol. 5, no. 24, pp. 12416–12425, Jun. 2017, doi: 10.1039/C7TA03150E.

[41] B. Roose *et al.*, “A Ga-doped SnO2 mesoporous contact for UV stable highly efficient perovskite solar cells,” *J Mater Chem A Mater*, vol. 6, no. 4, pp. 1850–1857, Jan. 2018, doi: 10.1039/C7TA07663K.

[42] P. Zhu *et al.*, “Simultaneous Contact and Grain-Boundary Passivation in Planar Perovskite Solar Cells Using SnO2-KCl Composite Electron Transport Layer,” *Adv Energy Mater*, vol. 10, no. 3, Jan. 2020, doi: 10.1002/AENM.201903083.

Chapter 02
Literature Review

The continued progression of perovskite solar cells as a promising technology for renewable energy generation relies on the optimization of their individual components. Among these, the electron transport layer plays a critical role in extracting and transporting photogenerated electrons, reducing recombination losses, and improving overall device performance. This review aims to provide a comprehensive understanding of the impact of most common ETL materials including TiO_2, SnO_2 and ZnO on PSC performance, with reference to key research articles. The review also presents a comprehensive literature review of different deposition techniques, and modification methods specifically applied for the development of SnO_2 ETLs for PSCs, focusing on elemental doping, bulk modification, and surface modification. The review highlights the impact of these modifications on the performance of PSCs and provides insights into the underlying mechanism. A significant gap in the current understanding of modification of SnO_2 has been identified which presents an opportunity for further exploration and understanding of SnO_2 modification through La(III) doping and their potential impacts on ETL characteristics.

2.1 Performance of Perovskite Solar Cells with Traditional ETLs

2.1.1 TiO_2 as ETL

As discussed earlier in section 1.3.2, TiO_2 is renowned for its exceptional electron mobility that ensures efficient electron transport from the perovskite layer to the electrode. Its bandgap is also well-aligned with the perovskite active layer, facilitating efficient electron-hole separation. Furthermore, TiO_2's robust chemical stability adds to the overall resilience of the PSC, and its environmental compatibility, owing to its non-toxic nature, makes it a preferred choice.

Jeon and coworkers demonstrated that using solvent engineering to deposit a mesoporous TiO_2 ETL can lead to an improved power conversion efficiency (PCE) of 16.2% in PSCs with almost no hysteresis [1]. By employing a vacuum flash-assisted solution process for

depositing a mesoporous TiO_2 ETL, Li et al. achieved PCEs of up to 20.5% for PSCs with large active areas exceeding 1 cm^2 with excellent reproducibility [2].

2.1.2 ZnO as ETL

ZnO also has properties conducive to efficient PSC performance. It possesses an excellent electron transport capacity and can be easily synthesized using various methods. Its wide bandgap and suitable conduction band level align well with perovskite materials, enabling efficient charge extraction and reduction in recombination losses. Additionally, the ability of ZnO to enhance light harvesting due to its scattering effect is a beneficial trait for PSCs.

Hu et al. demonstrated the effectiveness of sequential deposition of $CH_3NH_3PbI_3$ on planar ZnO as an ETL, achieving a PCE of 14.53% in PSCs. The devices demonstrated enhanced stability for over 20 days under ambient conditions [3]. Zhang et al. used a room-temperature solution process to develop a pinhole-free, surface-nanostructured ZnO ETL for flexible PSCs, achieving a PCE of 13.75% with good stability and reproducibility and reduced hysteresis [4]. Jia and team focused on interface engineering of the ZnO ETL in PSCs, which resulted in a PCE of >20% with improved growth of perovskite layer over ZnO ETL [5].

2.2 Performance of Perovskite Solar Cells with SnO_2

Tin dioxide has emerged as a popular choice for ETL in PSCs due to its favorable properties, such as wide bandgap, high electron mobility, and excellent chemical stability. Ke et al. demonstrated the effectiveness of low-temperature solution-processed SnO_2 as an alternative ETL in PSCs, achieving a PCE of 16.2% with excellent electron mobilities [6]. By utilizing SnO_2 as the ETL in a planar PSC, Jiang et al. achieved an impressive PCE of ~20% for a FAI-based perovskite solar cell [7]. The device had reduced charge accumulation at ETL/ Perovskite interface. Wang et al. and co-authors employed low-temperature (<100° C) plasma-enhanced atomic layer deposition to create SnO_2 ETLs, achieving a high PCE of 18% in planar PSCs [8].

The performance of SnO_2-based ETLs can be further enhanced by employing various modification strategies. This section offers an extensive analysis of various deposition

approaches and modification techniques employed for SnO2 ETLs in PSCs, with a particular emphasis on elemental doping, bulk alteration, and surface modification.

2.3 Effective Deposition Techniques and Surface Modification Approaches for ETLs

2.3.1 Deposition Techniques

The performance of SnO_2-based ETLs in PSCs is highly influenced by their morphological, structural, and electrical properties. These properties can be tailored by employing different deposition techniques during the fabrication process. This section provides an extensive review of various deposition methods that researchers have used to deposit SnO_2 thin films, along with their impact on the overall performance of PSCs**.**

2.3.1.1 Sol-Gel Process

The sol-gel process is a solution-based deposition technique that involves the formation of a colloidal suspension (sol), followed by gelation, aging, and drying to form a solid gel film. This film can then be heat-treated to convert it into the desired metal oxide ETL material. The sol-gel process offers good control over film thickness and morphology, as well as compatibility with low-temperature processing [9].

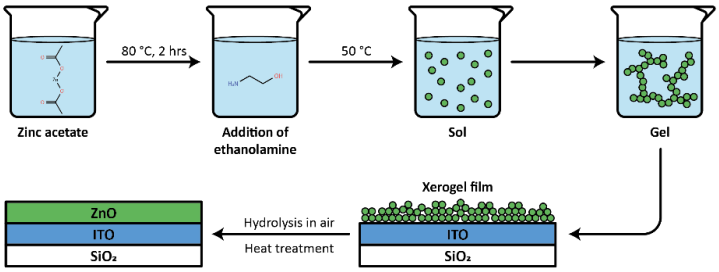

Figure 2.1. Sequential illustration of sol-gel process for deposition of thin films [10]

Numerous studies have been conducted on the synthesis and optimization of SnO_2 as an electron transport layer (ETL) in perovskite solar cells (PSCs). In 2015, Ma et al. prepared a SnO_2 organic solution using $SnCl_2 \cdot 2H_2O$ dissolved in ethyl alcohol, resulting in a PCE of 7.43% [11]. Yan et al. studied the effect of annealing temperatures on $SnCl_2$-based sol-gel and reported that low-temperature SnO_2 showed better performance than high-temperature SnO_2 [12]. They optimized the SnO_2 ETL using $SnCl_2 \cdot 2H_2O$ in ethanol,

achieving a PCE of 17.21%. In 2018, Jen et al. synthesized SnO_2 nanocrystals through a hydrothermal method and obtained a PCE of 18.80% [13]. In a similar approach, Jiu et al. (2016) enhanced the PCE from 13.2% to 19.7% in an inverted structure by incorporating SnO_2 nanoparticles into $PC_{61}BM$ [14]. In 2017, Wang et al. proposed a low-temperature (below 80ºC) method to synthesize SnO_2 nanocrystals [15]. Jiang et al. in 2016, achieved a PCE of 19.90% using a commercially available SnO_2 colloid precursor and further improved the efficiency to 21.6% by optimizing the PbI_2 passivation layer [16][17]. In 2019, Tan et al. combined KCl with SnO_2 nanoparticles and obtained an efficiency PCE of 22.2% by passivating the ETL/perovskite interface trap centers. These studies highlight the significance of SnO_2 optimization in achieving high-performance PSCs [18].

2.3.1.2 Chemical Bath Deposition

Chemical bath deposition (CBD) is a low-cost, simple, and versatile technique used for depositing thin films of various materials onto substrates at very low temperature (>100˚C) [9]. This method is particularly suitable for depositing semiconductors, insulators, and metal oxides. The process involves immersing a substrate into an aqueous solution containing metal ions and appropriate complexing agents, which results in a controlled chemical reaction that precipitates the desired material onto the substrate surface.

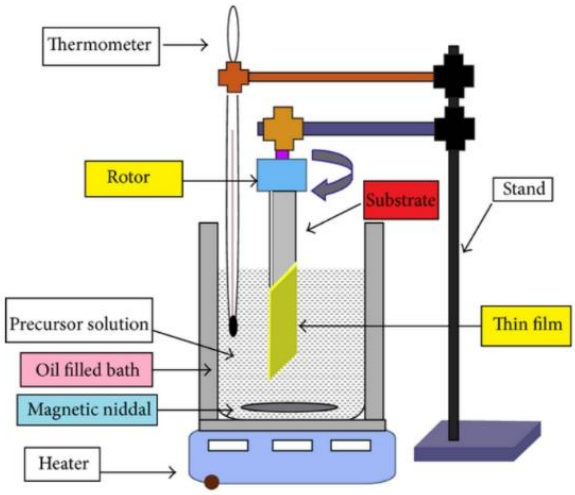

Figure 2.2. Thin film deposition by chemical bath deposition [19]

The deposition process is typically driven by factors such as pH, temperature, concentration of reactants, and reaction time. By carefully controlling these parameters,

the properties of the deposited thin film, such as thickness, uniformity, composition, and crystallinity, can be tailored to meet specific requirements. CBD is widely used in various applications, including solar cells, sensors, and optoelectronic devices, due to its low cost, scalability, and ability to produce high-quality thin films at relatively low temperatures.

CBD is a method of depositing thin films by immersing a substrate in a solution containing the precursor of the desired material, allowing the film to form through a chemical reaction. Hagfeldt et al. used CBD in combination with spin coating to deposit a bilayer of SnO_2 ETLs, which resulted in an impressive efficiency of 21% [14]. Later, Snaith et al. adopted the same approach for their wide-bandgap PSCs, which yielded a PCE of 17% [20]. Zhong and his team also used CBD to prepare compact SnO_2 ETLs, which led to a high PCE output of 20.56% in a small area and 15.76% in a 6x6 cm^2 submodule [21]. Moreover, they successfully demonstrated the potential of large-area deposition using CBD by reporting a 10x10 cm^2 module with a PCE of 17.82% [22]. In addition, doped SnO_2 ETLs were also achieved using CBD by dissolving chemicals into the bath solution. Anaraki et al. reported the successful deposition of Nb-doped SnO_2 ETLs by CBD, which resulted in a champion PCE of 20.5% [23]. Furthermore, Zhan et al. developed Ta-doped SnO_2 ETLs using CBD, which achieved a PCE of 20.80% [24]. These findings demonstrate the potential of CBD as a reliable and cost-effective technique for the deposition of high-quality ETLs in PSCs, with the added advantage of being scalable to large-area devices.

2.3.1.3 Atomic Layer Deposition

ALD is a vapor-phase deposition technique that involves the sequential exposure of a substrate to gas-phase precursors, resulting in the deposition of a monolayer of material in each cycle. ALD offers excellent control over film thickness (in angstrom) and composition, as well as superior conformality, making it particularly suitable for depositing ultrathin and pinhole-free metal oxide ETLs [25].

Atomic Layer Deposition (ALD) is a thin film deposition technique that has been extensively used for the development of efficient and stable Perovskite Solar Cells (PSCs). One study by Baena et al. (2015) successfully deposited a 15 nm-thick layer of SnO_2 ETL

in PSCs using a low-temperature ALD process at around 120°C, resulting in a high PCE of 18.4% with a record high open-circuit voltage (V_{oc}) of 1.19 V [27].

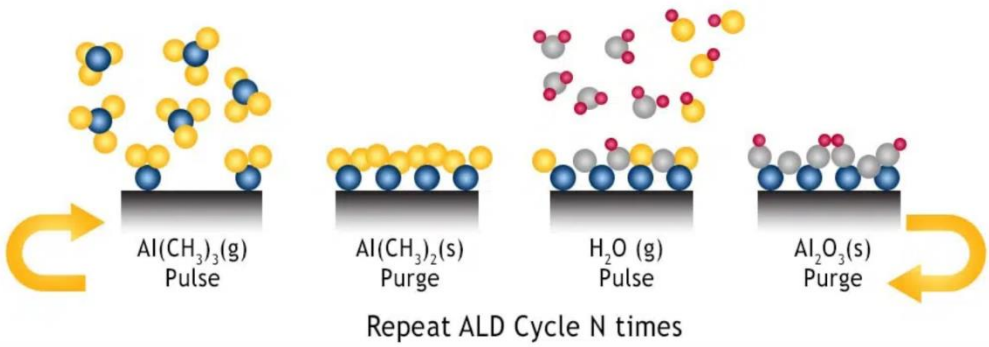

Figure 2.3. Atomic layer deposition cycle for thin film deposition [26]

ALD has also been utilized to deposit other ETL materials, such as ZnO, TiO_2, and Al_2O_3, which have shown improved device performance and stability. In a study by Wang et al. (2016), a highly uniform and conformal SnO_2 ETL layer was deposited on a perovskite absorber using PEALD, leading to improved PCE and device stability [28]. Subsequently in 2019, Wang et al. employed PEALD to deposit a SnO_2 ETL layer, which resulted in a high PCE of 20.3% and enhanced device stability [29]. These studies suggest the potential of ALD in producing high-performance and stable PSCs with improved uniformity and reproducibility.

2.3.1.4 Physical Vapor Deposition

Sputtering is one of the physical vapor depositions (PVD) techniques that involves the ejection of material from a target by bombarding it with high-energy particles, such as ions or electrons. The ejected material then condenses onto a nearby substrate, forming a high quality conductive thin film. Sputtering can be used to deposit a wide range of metal oxide ETL materials, such as TiO_2, SnO_2, and ZnO, with precise control over film thickness and composition [9].

In recent times, sputtered tin dioxide (SnO_2) has gained attention as an effective electron transport layer (ETL) material in perovskite solar cells (PSCs). A 2019 study by Qi and associates showcased high-quality SnO_2 films produced via room temperature sputtering, employing argon and oxygen gases. Creating an extremely oxidizing environment was

crucial for developing high-quality SnO_2 films, leading to PSCs with sputtered SnO_2 exhibiting an impressive power conversion efficiency (PCE) of 20.2% [31]. Similarly, Bai's team constructed a PSC submodule using magnetron sputtered SnO_2, achieving a PCE of 14.71% [32].

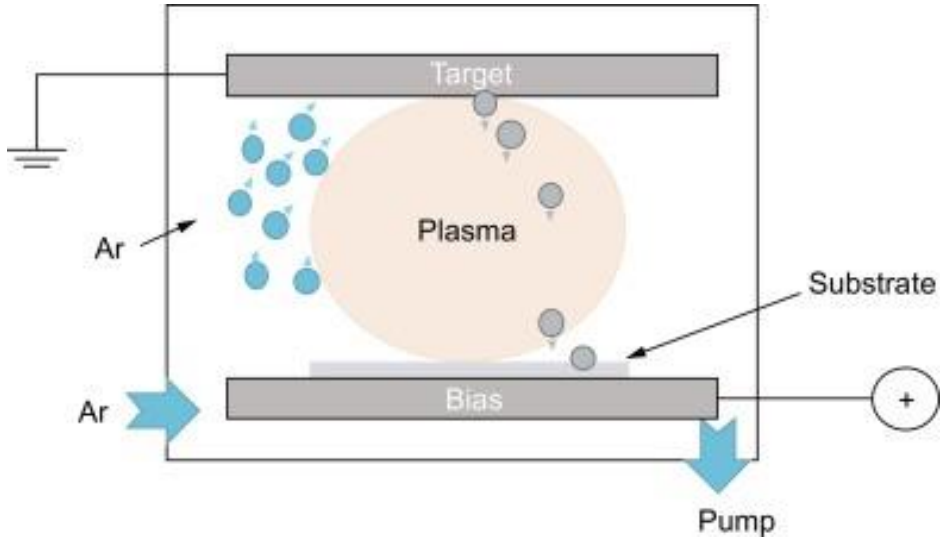

Figure 2.4. Sputtering Technique for thin film deposition [30]

Although evaporation is a prevalent physical vapor deposition (PVD) technique for thin film creation, its use with SnO_2 as an ETL in PSCs is less common. In 2020, Shi's group presented PSCs using e-beam evaporated SnO_2 ETL combined with a cesium-containing perovskite absorber, attaining a PCE of up to 18.2% [33]. Wang's research in 2021 also described a vacuum thermal evaporated SnO_2 as ETL, necessitating post-annealing to enhance the crystallinity of the evaporated SnO_2 and reach a PCE of 16.79% [34]. Additionally, Wang's team, in 2021, applied pulsed laser deposition (PLD) for depositing SnO_2 at room temperature without any post-annealing procedure. The resulting PSCs exhibited hysteresis-free PCEs of 17.29% and 14.0% on rigid and flexible substrates, respectively [35].

2.3.1.5 Spin Coating

Spin coating is a widely used technique for depositing thin films of metal oxides and organic materials at low cost. It involves the deposition of a liquid precursor or solution onto a substrate, followed by rapid spinning to spread the material evenly across the

surface. The spinning process also helps evaporate the solvent, leaving behind a thin and uniform film [36].

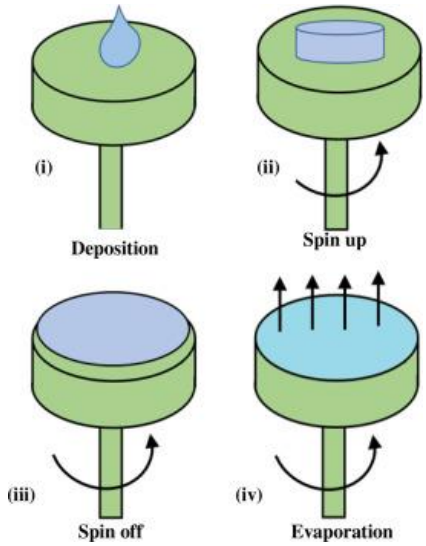

Figure 2.5. Sequential spin coating technique [37]

Gnachev et al. (2020) demonstrated the efficiency of the spin-coating technique in achieving uniform and compact SnO_2 films. The study found that the spin speed, solution concentration, and post-treatment significantly affect the film's morphological and optical properties, thereby influencing the device performance and yielding PCE up to 21% [38]. Furthermore, the study by Hoang et al. focused on the post-spin-coating treatment, specifically annealing, of the Ni: SnO_2 film. They reported that annealing at the appropriate temperature resulted in improved electron mobility and reduced defect density and improved particle size 3-5 nm, which contributed to an overall increase in device performance [39]. A study by park et al. (2023) highlighted the characteristics of spin coated SnO_2 for PSCs which demonstrated improved wettability along with well aligned energy band with perovskite [40].

2.3.2 Modification of SnO_2 ETL

SnO_2 as an electron transport layer (ETL) in perovskite solar cells (PSCs) can be modified in various ways to improve its properties and enhance the performance of the solar cells. Some of the modification techniques include elemental doping, bulk blending, and surface modification.

2.3.2.1 Elemental doping

SnO_2 can be modified by adding small amounts of other elements, such as fluorine, indium, antimony, or zinc, into the SnO_2 lattice during synthesis. The added elements can modify the electronic properties of SnO_2, such as its bandgap, work function, and charge carrier concentration. For example, adding fluorine can increase the electron concentration, while adding indium or antimony can increase the electron mobility. This can improve the efficiency of charge transfer between the perovskite layer and the ETL, leading to higher device performance.

a) P type doping

In the process of p-type doping, lower-valence cations such as Li^{+}, Mg^{2+}, Ru^{2+}, Zn^{2+}, Co^{3+}, Ga^{3+}, and Eu^{3+} are used to replace the tetravalent tin (Sn) sites. This type of doping in n-type semiconductors is known as compensatory doping, which diminishes the electron concentration within the conduction band (CB) of the semiconductor, subsequently decreasing the film's conductivity. However, for applications in perovskite solar cells (PSCs), an appropriately reduced electron concentration in the CB can effectively mitigate charge recombination. Introducing p-type dopants into SnO_2 ETL can enhance its electrical properties and shift the fermi level downwards, thereby boosting the overall efficiency of PSCs. For instance, Zhou et al. (2019) investigated the impact of gallium (Ga^{3+}) doping on SnO_2 ETL and found that it significantly improved the PCE of PSCs due to reduced charge recombination and enhanced charge extraction with a PCE of 18.18% [41]. Likewise, Mazumder et al. (2012) reported the enhancement of PCE in PSCs by incorporating magnesium (Mg^{+2}) as a p-type dopant into SnO_2 ETL through sol-gel, resulting in improved optoelectronic properties and reduced hysteresis with downward shift of fermi level [42].

Additionally, Zhou et al. (2020) demonstrated the effectiveness of incorporating copper (Cu^{2+}) dopants in SnO_2 ETL, leading to increased PCE (>21%) due to better carrier mobility, better energy band alignment and reduced charge recombination [43]. These findings suggest that the modification of SnO_2 ETL through p-type elemental doping holds great potential in optimizing the performance of PSCs. Further research in the realm of p-type elemental doping in SnO_2 ETL has been conducted by various groups. For example,

Chen et al. (2017) explored the effect of aluminum (Al^{3+}) doping on SnO_2 ETL and discovered enhanced PCE (~12.01%) and V_{oc} (1.03V) in PSCs due to improved charge extraction and reduced recombination [44]. In another study, Park et al. (2022) reported significant improvements in the performance of PSCs by introducing rubidium (Ru^{2+}) dopants into SnO_2 ETL, which led to better carrier mobility and reduced trap densities, reduced defect densities and morphological characteristics with a remarkable PCE of 22% [45]. Additionally, Kim et al. (2016) investigated the impact of lithium (Li^{+}) doping on SnO_2 ETL and observed improvements in PCE of flexible PSCs reaching 18.2% [40], mainly attributed to the enhanced electron transport properties due to the shifted fermi level. Finally, Zhang et al. (2019) demonstrated the benefits of introducing yttrium (Y^{3+}) dopants into SnO_2 ETL through solvothermal route, resulting in PSCs with improved charge extraction and PCE of 20.71% with minor hysteresis [46]. These studies showcase the potential of p-type elemental doping in SnO_2 ETL as a viable approach to optimize PSC performance.

b) N-type Doping

The replacement of tetravalent Sn sites with cations that possess higher valence states, like Ta^{5+}, Mo^{5+}, Sb^{5+}, and Nb^{5+}, can lead to n-type doping. This process results in an increase in electron concentration in the SnO_2 film, which can enhance electron transport and shift the Fermi level upwards. For example, Tantalum (Ta^{5+}) doped SnO_2 ETLs were shown to exhibit increased electron mobility and reduced series resistance, leading to a boosted PCE of 20.8% in comparison to pristine SnO_2-based PSCs (18.5%) [47]. Similarly, Anaraki et al. demonstrated CBD deposited Nb-doped SnO_2 ETLs with improved electron transport and reduced charge recombination, resulting in stabilized PCEs of up to 20.1%, significantly higher than that of undoped SnO_2 [48]. Furthermore, in 2019 Mo-doped SnO_2 ETLs have been reported by Bahadur et al. to provide enhanced electron extraction and reduced trap states with a shifted fermi level, contributing to a notable increase in PCE (10.52%) compared to pristine SnO_2 ETL-based devices (8.5%) [49]. Sb-doped SnO_2 ETLs have been studied for their ability to improve the overall performance of PSCs. Kim et al. (2011) reported that Sb-doped SnO_2 ETLs led to an enhanced electron extraction and transport, as well as a reduced recombination rate, which consequently increased the PCE of PSCs [50]. Moreover, the stability of the PSCs was also improved with the

incorporation of Sb dopants. In 2022 F-doped SnO_2 ETLs have been reported by Luo et al. to provide enhanced electron extraction and reduced trap states with a shifted fermi level, lower defect densities, better energy level alignment contributing to a notable increase in PCE (22.12%), maintaining up to 80% stability against moisture [51]. These studies highlight the promising role of n-type elemental doping in SnO_2 ETLs for optimizing the overall performance of PSCs. The improved device performance achieved through elemental doping underscores the importance of further research into the development of advanced ETLs and PSCs with higher efficiency and stability.

2.3.2.2 Bulk Blending

SnO_2 can be modified by blending it with other carbon-based materials or organic molecules. This can improve the overall properties of the ETL, such as charge transport and conductivity.

a) Bulk blending with carbon materials

Various strategies to improve the performance and stability of perovskite solar cells by modifying tin dioxide (SnO_2) electron transport layers through bulk blending. Efficient ETLs are essential for promoting carrier separation, electron extraction, and influencing the nucleation and growth of perovskite layers in PSCs. In one study (Gao et al., 2021) crystalline polymeric carbon nitrides (cPCN) were introduced to regulate the electronic properties of SnO_2 nanocrystals, resulting in SnO_2-cPCN composited ETLs with enhanced charge transport and perovskite layers with decreased grain boundaries. This approach led to a power conversion efficiency (PCE) of 23.17%, with higher stability compared to pristine SnO_2 devices [52]. Zhang et al. in 2020 incorporated graphdiyne (GDY) into the SnO_2 ETL to optimize electron extraction rates and interface engineering. This modification resulted in a high-quality perovskite film with diminished grain boundaries and lower defect density, as well as interfacial passivation of Pb-I anti-site defects [53]. Xie et al. in 2017 involved treating SnO_2 films with a small amount of graphene quantum dots (GQDs) to improve the electronic properties of SnO_2. The improved conductivity of SnO_2 in this strategy led to enhanced electron extraction efficiency and reduced recombination at the ETL/perovskite interface. Devices fabricated with SnO_2:GQDs achieved an average PCE of 19.2 ± 1.0% [54]. SnO_2/graphitic carbon nitride (g-C_3N_4)

quantum dot nanocomposite was designed as the functional ETL to enhance interfacial charge dynamics and improve PSC performance. This hybrid ETL resulted in a maximum PCE of 22.13% with negligible hysteresis and long-term stability [55]. A hybrid ETL of SnO_2 and carbon nanotubes (CNTs) was fabricated through thermal decomposition. The addition of CNTs improved the conductivity and reduced the trap-state density of SnO_2 films, leading to a hysteresis-free PSC with a high efficiency of 20.33% [56].

b) Bulk blending with organic molecules

The table below shows various photovoltaic parameters for PSCs employing organic molecules bulk blended with SnO_2.

Table 1 Bulk blended SnO_2 using organic molecules

Modifier	**Jsc (mA/cm^2)**	**Voc (V)**	**FF**	**PCE %**	**Ref.**
Polyethylene glycol	23.12	1.1	0.75	19.71	[57]
2,2,2-Trifluoroethanol	22.62	1.09	0.77	19.2	[58]
Ethylene diamine tetraacitic acid (EDTA)	22.92	1.08	0.76	18.7	[59]
Polyethyleneimine (PEIE)	22.79	1.1	0.75	18.9	[60]
P-amino benzene sulfonic acid (ABSA)	22.39	1.1	0.73	18.02	[61]
Choline- chlorine	22.26	1.07	0.73	16.83	[62]

2.3.2.3 Surface Modification

SnO_2 can also be modified by treating its surface with various functional groups including carbon-based materials, organic molecules or metal oxides. This can improve its surface properties, such as wettability, charge extraction, and electron injection.

a) Surface modification with carbon materials

Researchers have explored different strategies to enhance the performance and stability of perovskite solar cells by modifying tin dioxide (SnO_2) electron transport layers (ETLs) through surface modification with carbon materials.

Table 2 Surface Modified SnO_2 using carbon materials.

Modification	Key benefits	PCE %	FF	Ref.
Phenyl-C_{61}-butyric acid methyl ester (PCBM) and [6,6]-Phenyl-C_{61}-butyric acid (PCBA)	Reduced defects, enhanced electron mobility	18.8	0.74	[63]
Fulleropyrrolidine dimers	Superior stability, efficiency improvements	22.3	0.71	[64]
C_9 fullerene derivative	Enhanced carrier extraction, improved film quality	21.3	0.78	[65]
C_{60} pyrrolidine tris-acid (CPTA)-modified SnO_2 ETL and 6,6-Phenyl C_{61}-butyric acid methyl ester ($PC_{61}BM$)	Enhanced electron injection, reduced recombination	>19.0	0.82	[66]
C_{60} pyrrolidine tris-acid (CPTA)	High efficiency in Sn-based PSCs	7.4	0.79	[67]
CPTA modified SnO_2 on polyethylene naphthalate	Improved carrier selectivity, flexible PSCs	18.36	0.67	[68]

b) Surface modification using organic molecules

In recent years, numerous studies have been conducted to improve the power conversion efficiency (PCE) and stability of perovskite solar cells through interfacial engineering. One such study by Smith et al. (2022) focused on using guanidinium (GA) chloride to modify the surface of tin dioxide (SnO_2) nanoparticles, commonly employed as an electron transfer material in PSCs [69]. The researchers found that GA modification effectively reduced the energy barrier at the SnO_2/perovskite interface, resulting in an increased PCE from 15.33% to 18.46% and a maximum fill factor of 80%. The strong coupling between GA and adsorbed oxygen species was identified as the primary factor responsible for this performance enhancement. In a similar vein, Johnson et al. recently utilized a dopamine (DA) self-assembled monolayer (SAM) to modify the SnO_2/perovskite interface in organic-inorganic PSCs [70]. This approach improved the

PCE from 14.05% to 16.65% by enhancing the quality of perovskite films, resulting in better carrier transport and reduced charge recombination. These findings suggest that DA SAM modification holds a promise for producing more efficient and stable PSCs. An innovative study by Lee et al. explored the use of creatine, as a cathode interfacial layer on the SnO_2 layer in PSCs [71]. This naturally occurring compound, often consumed by athletes for energy, strengthened charge extraction by forming interface dipoles and reducing the work function. Furthermore, it passivated defects in the perovskite layer, contributing to a significant increase in PCE. Triple cation-based perovskite devices achieved the highest PCE of 20.8% and retained 90% of it after 50 days, while formamidinium-based perovskite devices reached 22.1% PCE. This innovative application of creatine highlights its potential as an interfacial layer in PSCs and suggests that other essential amino acids may also be explored for similar purposes.

c) Surface modification by metal oxides

Metallic oxides such as titanium dioxide (TiO_2), zinc oxide (ZnO), tungsten oxide (WO_x), indium oxide (In_2O_3), and lead oxide (PbO) possess distinct characteristics that make them ideal candidates for electron transport layer (ETL) applications in perovskite solar cells (PSCs) alongside tin oxide (SnO_2). The integration of SnO_2 with various metal oxides can be beneficial in customizing the ETL's surface structure, establishing graduated energy levels, and/or fine-tuning the interfacial contact. This can result in enhanced solar cell performance. A synopsis of the photovoltaic efficiency of representative PSCs utilizing metal oxide modified SnO_2 as the ETL is provided in Table below.

Table 3 Device parameters for Metal oxide modified SnO_2.

Structure of ETL	Jsc (mA/cm^2)	Voc (V)	FF	PCE %	Ref.
SnO_2/ MgO	21.3	1.10	0.64	15.2	[72]
SnO_2/ TiO_2	18.4	0.65	0.52	6.2	[73]
SnO_2/ ZnO	14.7	1.06	0.75	11.9	[74]
SnO_2/ Eu: WOx	23.3	1.71	0.73	19.03	[75]
In_2O_3/ SnO_2	24.2	1.13	0.78	21.42	[76]
SnO_2/ PbO	20.9	1.11	0.72	16.91	[77]
MgO/ SnO_2	21.6	1.07	0.71	16.11	[78]

Rare earth metals are considered good doping candidates as they possess unfilled 4f electronic shell [79], [80], which gives La its exceptional optoelectronic characteristics. When Lanthanide (La) is integrated into ETL, it can influence ETL's electrical, optical and stability aspects [79]. Despite the growing interest in perovskite solar cells (PSCs), research on lanthanum-doped tin oxide (La:SnO_2) ETLs in conjunction with cesium-doped methylammonium lead iodide absorber layer ($Cs_xMA_{1-x}PbI_3$) remains limited, particularly under ambient conditions.

In this investigation, we explore various factors that influence the properties of tin dioxide (SnO_2) by incorporating La (III) for use as an electron transport layer in PSCs. Our findings demonstrate that the introduction of lanthanum improves SnO_2 thin film crystallinity during the annealing process. Lanthanum-doped films exhibit superior characteristics compared to undoped SnO_2, such as increased average transmittance and conductivity at ETL-perovskite contact. The incorporation of lanthanum facilitates injection and transfer of charges at the interface. Moreover, the perovskite layer deposited on the lanthanum doped SnO_2 (La:SnO_2) demonstrates reduced grain boundary density, larger grain sizes, and enhanced hydrophobicity, which contribute to an improved fill factor (FF) and increased device stability under ambient conditions. As a result, La:SnO_2 ETLs show great potential for integration into planar PSCs, offering superior light-soaking capabilities.

Summary

In summary, this chapter provided an extensive review of various deposition techniques and modification methods employed for SnO_2 ETLs in PSCs, with a focus on elemental doping (P-type and N-type), bulk blending and surface modification, carbon materials, organic molecule incorporation, and metal oxide modification. By examining the effects of these modifications on PSC performance and the underlying mechanisms, the review sheds light on the potential for further optimization of SnO_2-based ETLs. The discussion encompassed different strategies and materials used in each modification method, highlighting their respective advantages, limitations, and impacts on device performance. The chapter also provides an insight into the research gap and the steps taken towards the understanding of La(III) doped SnO_2.

References

[1] N. J. Jeon, J. H. Noh, Y. C. Kim, W. S. Yang, S. Ryu, and S. Il Seok, "Solvent engineering for high-performance inorganic-organic hybrid perovskite solar cells," *Nat Mater*, vol. 13, no. 9, pp. 897–903, 2014, doi: 10.1038/NMAT4014.

[2] X. Li *et al.*, "A vacuum flash-assisted solution process for high-efficiency large-area perovskite solar cells," *Science*, vol. 353, no. 6294, pp. 58–62, Jul. 2016, doi: 10.1126/SCIENCE.AAF8060.

[3] Z. Putao *et al.*, "Enhanced performance of ZnO based perovskite solar cells by Nb 2 O 5 surface passivation," 2018.

[4] J. Han, H. Kwon, E. Kim, D. W. Kim, H. J. Son, and D. H. Kim, "Interfacial engineering of a ZnO electron transporting layer using self-assembled monolayers for high performance and stable perovskite solar cells," *J Mater Chem A Mater*, vol. 8, no. 4, pp. 2105–2113, Jan. 2020, doi: 10.1039/C9TA12750J.

[5] X. Wu *et al.*, "ZnO electron transporting layer engineering realized over 20% efficiency and over 1.28 V open-circuit voltage in all-inorganic perovskite solar cells," *EcoMat*, vol. 4, no. 4, p. e12192, Jul. 2022, doi: 10.1002/EOM2.12192.

[6] W. Ke *et al.*, "Lowerature solution-processed tin oxide as an alternative electron transporting layer for efficient perovskite solar cells," *J Am Chem Soc*, vol. 137, no. 21, pp. 6730–6733, Jun. 2015, doi: 10.1021/JACS.5B01994/SUPPL_FILE/JA5B01994_SI_001.PDF.

[7] Q. Jiang *et al.*, "Enhanced electron extraction using SnO2 for high-efficiency planar-structure HC(NH2)2PbI3-based perovskite solar cells," *Nature Energy 2016 2:1*, vol. 2, no. 1, pp. 1–7, Nov. 2016, doi: 10.1038/nenergy.2016.177.

[8] C. Wang *et al.*, "Low-temperature plasma-enhanced atomic layer deposition of tin oxide electron selective layers for highly efficient planar perovskite solar cells," *J Mater Chem A Mater*, vol. 4, no. 31, pp. 12080–12087, Aug. 2016, doi: 10.1039/C6TA04503K.

[9] A. Uddin and H. Yi, "Progress and Challenges of SnO2 Electron Transport Layer for Perovskite Solar Cells: A Critical Review," *Solar RRL*, vol. 6, no. 6. John Wiley and Sons Inc, Jun. 01, 2022. doi: 10.1002/solr.202100983.

[10] X. Guo *et al.*, "Synthesis and application of several sol–gel-derived materials via sol–gel process combining with other technologies: a review," *J Solgel Sci Technol*, vol. 79, no. 2, pp. 328–358, Aug. 2016, doi: 10.1007/S10971-015-3935-6.

[11] K. Wang *et al.*, "Low-temperature and solution-processed amorphous WOX as electron-selective layer for perovskite solar cells," *Journal of Physical Chemistry Letters*, vol. 6, no. 5, pp. 755–759, Mar. 2015, doi: 10.1021/ACS.JPCLETT.5B00010/SUPPL_FILE/JZ5B00010_SI_001.PDF.

[12] W. Ke *et al.*, "Lowerature solution-processed tin oxide as an alternative electron transporting layer for efficient perovskite solar cells," *J Am Chem Soc*, vol. 137, no. 21, pp. 6730–6733, Jun. 2015, doi: 10.1021/JACS.5B01994/SUPPL_FILE/JA5B01994_SI_001.PDF.

[13] X. Liu, C. C. Chueh, Z. Zhu, S. B. Jo, Y. Sun, and A. K. Y. Jen, "Highly crystalline Zn2SnO4 nanoparticles as efficient electron-transporting layers toward stable inverted and flexible conventional perovskite solar cells," *J Mater Chem A Mater*, vol. 4, no. 40, pp. 15294–15301, Oct. 2016, doi: 10.1039/C6TA05745D.

[14] Q. Dong, Y. Shi, C. Zhang, Y. Wu, and L. Wang, "Energetically favored formation of SnO2 nanocrystals as electron transfer layer in perovskite solar cells with high efficiency exceeding 19%," *Nano Energy*, vol. 40, pp. 336–344, Oct. 2017, doi: 10.1016/J.NANOEN.2017.08.041.

[15] Y. Wang *et al.*, "Performance Enhancement of Inverted Perovskite Solar Cells Based on Smooth and Compact PC61BM:SnO2 Electron Transport Layers," *ACS Appl Mater Interfaces*, vol. 10, no. 23, pp. 20128–20135, Jun. 2018, doi: 10.1021/ACSAMI.8B03444.

[16] Q. Jiang *et al.*, "Enhanced electron extraction using SnO2 for high-efficiency planar-structure HC(NH2)2PbI3-based perovskite solar cells," *Nature Energy 2016 2:1*, vol. 2, no. 1, pp. 1–7, Nov. 2016, doi: 10.1038/nenergy.2016.177.

[17] Q. Jiang *et al.*, "Planar-Structure Perovskite Solar Cells with Efficiency beyond 21%," *Advanced Materials*, vol. 29, no. 46, p. 1703852, Dec. 2017, doi: 10.1002/ADMA.201703852.

[18] "Comprehensive insights into defect passivation and charge dynamics for FA0.8MA0.15Cs0.05PbI2.8Br0.2 perovskite solar cells. Applied Physics Letters, 117(1), 013503 | 10.1063/5.0010705." https://doi.org/10.1063/5.0010705 (accessed May 09, 2023).

[19] "Figure 8 | Research and Development Aspects on Chemical Preparation Techniques of Photoanodes for Dye Sensitized Solar Cells." https://www.hindawi.com/journals/ijp/2014/518156/fig8/ (accessed May 11, 2023).

[20] D. P. McMeekin *et al.*, "A mixed-cation lead mixed-halide perovskite absorber for tandem solar cells," *Science*, vol. 351, no. 6269, pp. 151–155, Jan. 2016, doi: 10.1126/SCIENCE.AAD5845.

[21] T. Bu *et al.*, "A novel quadruple-cation absorber for universal hysteresis elimination for high efficiency and stable perovskite solar cells," *Energy Environ Sci*, vol. 10, no. 12, pp. 2509–2515, Dec. 2017, doi: 10.1039/C7EE02634J.

[22] T. Bu *et al.*, "Dynamic antisolvent engineering for spin coating of 10 × 10 cm2 perovskite solar module approaching 18%," *Solar RRL*, vol. 4, no. 2, p. 1900263, Feb. 2020, doi: 10.1002/SOLR.201900263.

[23] E. H. Anaraki *et al.*, "Highly efficient and stable planar perovskite solar cells by solution-processed tin oxide," *Energy Environ Sci*, vol. 9, no. 10, pp. 3128–3134, Oct. 2016, doi: 10.1039/C6EE02390H.

[24] Q. Liu *et al.*, "Effect of tantalum doping on SnO2 electron transport layer via low temperature process for perovskite solar cells," *Appl Phys Lett*, vol. 115, no. 14, Sep. 2019, doi: 10.1063/1.5118679.

[25] Q. Jiang, X. Zhang, and J. You, “SnO2: A Wonderful Electron Transport Layer for Perovskite Solar Cells,” *Small*, vol. 14, no. 31. Wiley-VCH Verlag, Aug. 02, 2018. doi: 10.1002/smll.201801154.

[26] “WHAT IS PARTICLE ATOMIC LAYER DEPOSITION? - Forge Nano.” https://www.forgenano.com/what-is-particle-atomic-layer-deposition/ (accessed May 11, 2023).

[27] J. P. Correa Baena *et al.*, “Highly efficient planar perovskite solar cells through band alignment engineering,” *Energy Environ Sci*, vol. 8, no. 10, pp. 2928–2934, Oct. 2015, doi: 10.1039/C5EE02608C.

[28] C. Wang *et al.*, “Low-temperature plasma-enhanced atomic layer deposition of tin oxide electron selective layers for highly efficient planar perovskite solar cells,” *J Mater Chem A Mater*, vol. 4, no. 31, pp. 12080–12087, Aug. 2016, doi: 10.1039/C6TA04503K.

[29] C. Wang *et al.*, “Improving Performance and Stability of Planar Perovskite Solar Cells through Grain Boundary Passivation with Block Copolymers,” *Solar RRL*, vol. 3, no. 9, p. 1970085, Sep. 2019, doi: 10.1002/SOLR.201970085.

[30] K.-D. Bouzakis and N. Michailidis, “Physical Vapor Deposition (PVD),” *CIRP Encyclopedia of Production Engineering*, pp. 1308–1316, 2019, doi: 10.1007/978-3-662-53120-4_6489.

[31] L. Qiu *et al.*, “Scalable Fabrication of Stable High Efficiency Perovskite Solar Cells and Modules Utilizing Room Temperature Sputtered SnO2 Electron Transport Layer,” *Adv Funct Mater*, vol. 29, no. 47, p. 1806779, Nov. 2019, doi: 10.1002/ADFM.201806779.

[32] G. Bai *et al.*, “High performance perovskite sub-module with sputtered SnO2 electron transport layer,” *Solar Energy*, vol. 183, pp. 306–314, May 2019, doi: 10.1016/J.SOLENER.2019.03.026.

[33] T. Shi *et al.*, “Low-temperature fabrication of carbon-electrode based, hole-conductor-free and mesoscopic perovskite solar cells with power conversion

efficiency > 12% and storage-stability > 220 days," *Appl Phys Lett*, vol. 117, no. 16, p. 163501, Oct. 2020, doi: 10.1063/5.0025442/13463795/163501_1_ACCEPTED_MANUSCRIPT.PDF.

[34] Y. Wang, L. Yang, C. Dall'Agnese, G. Chen, A. J. Li, and X. F. Wang, "Spray-coated SnO2 electron transport layer with high uniformity for planar perovskite solar cells," *Front Chem Sci Eng*, vol. 15, no. 1, pp. 180–186, Feb. 2021, doi: 10.1007/S11705-020-1917-X/METRICS.

[35] Z. Chen *et al.*, "Bulk heterojunction perovskite solar cells based on room temperature deposited hole-blocking layer: Suppressed hysteresis and flexible photovoltaic application," *J Power Sources*, vol. 351, pp. 123–129, May 2017, doi: 10.1016/J.JPOWSOUR.2017.03.087.

[36] S. Huang, P. Li, J. Wang, J. C. C. Huang, Q. Xue, and N. Fu, "Modification of SnO2 electron transport Layer: Brilliant strategies to make perovskite solar cells stronger," *Chemical Engineering Journal*, vol. 439. Elsevier B.V., Jul. 01, 2022. doi: 10.1016/j.cej.2022.135687.

[37] B. S. Yilbas, A. Al-Sharafi, and H. Ali, "Surfaces for Self-Cleaning," *Self-Cleaning of Surfaces and Water Droplet Mobility*, pp. 45–98, 2019, doi: 10.1016/B978-0-12-814776-4.00003-3.

[38] H. Ren, X. Zou, J. Cheng, T. Ling, X. Bai, and D. Chen, "Facile solution spin-coating SnO2 thin film covering cracks of TiO2 hole blocking layer for perovskite solar cells," *Coatings*, vol. 8, no. 9, 2018, doi: 10.3390/COATINGS8090314.

[39] H. V. Quy and C. W. Bark, "Ni-Doped SnO2as an Electron Transport Layer by a Low-Temperature Process in Planar Perovskite Solar Cells," *ACS Omega*, vol. 7, no. 26, pp. 22256–22262, Jul. 2022, doi: 10.1021/acsomega.2c00965.

[40] M. Park, J. Y. Kim, H. J. Son, C. H. Lee, S. S. Jang, and M. J. Ko, "Low-temperature solution-processed Li-doped SnO2 as an effective electron transporting layer for high-performance flexible and wearable perovskite solar cells," *Nano Energy*, vol. 26, pp. 208–215, Aug. 2016, doi: 10.1016/J.NANOEN.2016.04.060.

[41] Z. Ma *et al.*, "Negligible hysteresis planar perovskite solar cells using Ga-doped SnO2 nanocrystal as electron transport layers," *Org Electron*, vol. 71, pp. 98–105, Aug. 2019, doi: 10.1016/J.ORGEL.2019.05.011.

[42] N. Mazumder, A. Bharati, S. Saha, D. Sen, and K. K. Chattopadhyay, "Effect of Mg doping on the electrical properties of SnO 2 nanoparticles," *Current Applied Physics*, vol. 12, no. 3, pp. 975–982, May 2012, doi: 10.1016/J.CAP.2011.12.022.

[43] X. Zhou *et al.*, "Solution-processed Cu-doped SnO2 as an effective electron transporting layer for High-Performance planar perovskite solar cells," *Appl Surf Sci*, vol. 584, p. 152651, May 2022, doi: 10.1016/J.APSUSC.2022.152651.

[44] H. Chen *et al.*, "Enhanced Performance of Planar Perovskite Solar Cells Using Low-Temperature Solution-Processed Al-Doped SnO2 as Electron Transport Layers," *Nanoscale Res Lett*, vol. 12, no. 1, pp. 1–6, Dec. 2017, doi: 10.1186/S11671-017-1992-1/FIGURES/4.

[45] S. Akin, "Hysteresis-Free Planar Perovskite Solar Cells with a Breakthrough Efficiency of 22% and Superior Operational Stability over 2000 h," *ACS Appl Mater Interfaces*, vol. 11, no. 43, pp. 39998–40005, Oct. 2019, doi: 10.1021/ACSAMI.9B13876/SUPPL_FILE/AM9B13876_SI_001.PDF.

[46] J. Song, W. Zhang, D. Wang, K. Deng, J. Wu, and Z. Lan, "Colloidal synthesis of Y-doped SnO2 nanocrystals for efficient and slight hysteresis planar perovskite solar cells," *Solar Energy*, vol. 185, pp. 508–515, Jun. 2019, doi: 10.1016/J.SOLENER.2019.04.084.

[47] Q. Liu *et al.*, "Effect of tantalum doping on SnO2 electron transport layer via low temperature process for perovskite solar cells," *Appl Phys Lett*, vol. 115, no. 14, p. 143903, Sep. 2019, doi: 10.1063/1.5118679/37736.

[48] E. Halvani Anaraki *et al.*, "Low-Temperature Nb-Doped SnO2 Electron-Selective Contact Yields over 20% Efficiency in Planar Perovskite Solar Cells," *ACS Energy Lett*, vol. 3, no. 4, pp. 773–778, Apr. 2018, doi: 10.1021/ACSENERGYLETT.8B00055/SUPPL_FILE/NZ8B00055_SI_001.PDF.

[49] J. Bahadur, A. H. Ghahremani, B. Martin, T. Druffel, M. K. Sunkara, and K. Pal, "Solution processed Mo doped SnO2 as an effective ETL in the fabrication of low temperature planer perovskite solar cell under ambient conditions," *Org Electron*, vol. 67, pp. 159–167, Apr. 2019, doi: 10.1016/J.ORGEL.2019.01.027.

[50] Y. S. Kim, B. K. Yu, D. Y. Kim, and W. B. Kim, "A hybridized electron-selective layer using Sb-doped SnO2 nanowires for efficient inverted polymer solar cells," *Solar Energy Materials and Solar Cells*, vol. 95, no. 10, pp. 2874–2879, Oct. 2011, doi: 10.1016/J.SOLMAT.2011.06.004.

[51] T. Luo, G. Ye, X. Chen, H. Wu, W. Zhang, and H. Chang, "F-doping-Enhanced Carrier Transport in the SnO2/Perovskite Interface for High-Performance Perovskite Solar Cells," *ACS Appl Mater Interfaces*, vol. 14, no. 37, pp. 42093–42101, Sep. 2022, doi: 10.1021/ACSAMI.2C11390/SUPPL_FILE/AM2C11390_SI_001.PDF.

[52] Z. Li *et al.*, "cPCN-Regulated SnO2 Composites Enables Perovskite Solar Cell with Efficiency Beyond 23%," *Nanomicro Lett*, vol. 13, no. 1, Dec. 2021, doi: 10.1007/s40820-021-00636-0.

[53] S. Zhang *et al.*, "Graphdiyne: Bridging SnO2 and Perovskite in Planar Solar Cells," *Angewandte Chemie - International Edition*, vol. 59, no. 28, pp. 11573–11582, Jul. 2020, doi: 10.1002/anie.202003502.

[54] J. Xie *et al.*, "Enhanced Electronic Properties of SnO2 via Electron Transfer from Graphene Quantum Dots for Efficient Perovskite Solar Cells," *ACS Nano*, vol. 11, no. 9, pp. 9176–9182, Sep. 2017, doi: 10.1021/acsnano.7b04070.

[55] J. Chen *et al.*, "Graphitic carbon nitride doped SnO2 enabling efficient perovskite solar cells with PCEs exceeding 22%," *J Mater Chem A Mater*, vol. 8, no. 5, pp. 2644–2653, 2020, doi: 10.1039/c9ta11344d.

[56] H. Tang *et al.*, "SnO2–Carbon Nanotubes Hybrid Electron Transport Layer for Efficient and Hysteresis-Free Planar Perovskite Solar Cells," *Solar RRL*, vol. 4, no. 1, Jan. 2020, doi: 10.1002/solr.201900415.

[57] J. Wei *et al.*, “SnO2-in-Polymer Matrix for High-Efficiency Perovskite Solar Cells with Improved Reproducibility and Stability,” *Advanced Materials*, vol. 30, no. 52, p. 1805153, Dec. 2018, doi: 10.1002/ADMA.201805153.

[58] Y. Luan *et al.*, “High-Performance Planar Perovskite Solar Cells with Negligible Hysteresis Using 2,2,2-Trifluoroethanol-Incorporated SnO2,” *iScience*, vol. 16, pp. 433–441, Jun. 2019, doi: 10.1016/j.isci.2019.06.004.

[59] D. Yang *et al.*, “High efficiency planar-type perovskite solar cells with negligible hysteresis using EDTA-complexed SnO2,” *Nature Communications 2018 9:1*, vol. 9, no. 1, pp. 1–11, Aug. 2018, doi: 10.1038/s41467-018-05760-x.

[60] X. Huang *et al.*, “Polyelectrolyte-Doped SnO2 as a Tunable Electron Transport Layer for High-Efficiency and Stable Perovskite Solar Cells,” *Solar RRL*, vol. 4, no. 1, p. 1900336, Jan. 2020, doi: 10.1002/SOLR.201900336.

[61] Y. Sun, J. Zhang, H. Yu, J. Wang, C. Huang, and J. Huang, “Mechanism of bifunctional p-amino benzenesulfonic acid modified interface in perovskite solar cells,” *Chemical Engineering Journal*, vol. 420, p. 129579, Sep. 2021, doi: 10.1016/J.CEJ.2021.129579.

[62] J. Yan, Z. Lin, Q. Cai, X. Wen, and C. Mu, “Choline Chloride-Modified SnO2Achieving High Output Voltage in MAPbI3Perovskite Solar Cells,” *ACS Appl Energy Mater*, vol. 3, no. 4, pp. 3504–3511, Apr. 2020, doi: 10.1021/ACSAEM.0C00038/SUPPL_FILE/AE0C00038_SI_001.PDF.

[63] X. Zhang *et al.*, “Energy Level Modification with Carbon Dot Interlayers Enables Efficient Perovskite Solar Cells and Quantum Dot Based Light-Emitting Diodes,” *Adv Funct Mater*, vol. 30, no. 11, Mar. 2020, doi: 10.1002/adfm.201910530.

[64] H. Wang *et al.*, “Chlorinated Fullerene Dimers for Interfacial Engineering Toward Stable Planar Perovskite Solar Cells with 22.3% Efficiency,” *Adv Energy Mater*, vol. 10, no. 21, Jun. 2020, doi: 10.1002/aenm.202000615.

[65] K. Liu *et al.*, “Fullerene derivative anchored SnO2 for high-performance perovskite solar cells,” *Energy Environ Sci*, vol. 11, no. 12, pp. 3463–3471, Dec. 2018, doi: 10.1039/c8ee02172d.

[66] W. Ke *et al.*, “Cooperative tin oxide fullerene electron selective layers for high-performance planar perovskite solar cells,” *J Mater Chem A Mater*, vol. 4, no. 37, pp. 14276–14283, 2016, doi: 10.1039/c6ta05095f.

[67] Z. Yang *et al.*, “SnO2-C60 Pyrrolidine Tris-Acid (CPTA) as the Electron Transport Layer for Highly Efficient and Stable Planar Sn-Based Perovskite Solar Cells,” *Adv Funct Mater*, vol. 29, no. 42, Oct. 2019, doi: 10.1002/adfm.201903621.

[68] M. Zhong, Y. Liang, J. Zhang, Z. Wei, Q. Li, and D. Xu, “Highly efficient flexible MAPbI3 solar cells with a fullerene derivative-modified SnO2 layer as the electron transport layer,” *J Mater Chem A Mater*, vol. 7, no. 12, pp. 6659–6664, 2019, doi: 10.1039/c9ta00398c.

[69] M. Yu *et al.*, “Effect of guanidinium chloride in eliminating O2-electron extraction barrier on a SnO2surface to enhance the efficiency of perovskite solar cells,” *RSC Adv*, vol. 10, no. 33, pp. 19513–19520, May 2020, doi: 10.1039/d0ra01501f.

[70] M. Hou, H. Zhang, Z. Wang, Y. Xia, Y. Chen, and W. Huang, “Enhancing Efficiency and Stability of Perovskite Solar Cells via a Self-Assembled Dopamine Interfacial Layer,” *ACS Appl Mater Interfaces*, vol. 10, no. 36, pp. 30607–30613, Sep. 2018, doi: 10.1021/acsami.8b10332.

[71] G. W. Kim, Y. Choi, H. Choi, J. Min, T. Park, and S. Song, “Novel cathode interfacial layer using creatine for enhancing the photovoltaic properties of perovskite solar cells,” *J Mater Chem A Mater*, vol. 8, no. 41, pp. 21721–21728, Nov. 2020, doi: 10.1039/d0ta08239b.

[72] J. Dagar, S. Castro-Hermosa, G. Lucarelli, F. Cacialli, and T. M. Brown, “Highly efficient perovskite solar cells for light harvesting under indoor illumination via solution processed SnO2/MgO composite electron transport layers,” *Nano Energy*, vol. 49, pp. 290–299, Jul. 2018, doi: 10.1016/J.NANOEN.2018.04.027.

[73] P. Wang *et al.*, "Gradient Energy Alignment Engineering for Planar Perovskite Solar Cells with Efficiency Over 23%," *Advanced Materials*, vol. 32, no. 6, p. 1905766, Feb. 2020, doi: 10.1002/ADMA.201905766.

[74] L. Yan *et al.*, "Interface Engineering for All-Inorganic CsPbI2Br Perovskite Solar Cells with Efficiency over 14%," *Advanced Materials*, vol. 30, no. 33, p. 1802509, Aug. 2018, doi: 10.1002/ADMA.201802509.

[75] X. Chen *et al.*, "Europium ions doped WOx nanorods for dual interfacial modification facilitating high efficiency and stability of perovskite solar cells," *Nano Energy*, vol. 80, p. 105564, Feb. 2021, doi: 10.1016/J.NANOEN.2020.105564.

[76] J. Dagar, S. Castro-Hermosa, G. Lucarelli, F. Cacialli, and T. M. Brown, "Highly efficient perovskite solar cells for light harvesting under indoor illumination via solution processed SnO2/MgO composite electron transport layers," *Nano Energy*, vol. 49, pp. 290–299, Jul. 2018, doi: 10.1016/J.NANOEN.2018.04.027.

[77] Z. Bi *et al.*, "High Shunt Resistance SnO2-PbO Electron Transport Layer for Perovskite Solar Cells Used in Low Lighting Applications," *Adv Sustain Syst*, vol. 5, no. 11, p. 2100120, Nov. 2021, doi: 10.1002/ADSU.202100120.

[78] J. Ma *et al.*, "MgO Nanoparticle Modified Anode for Highly Efficient SnO2-Based Planar Perovskite Solar Cells," *Advanced Science*, vol. 4, no. 9, p. 1700031, Sep. 2017, doi: 10.1002/ADVS.201700031.

[79] Z. Xu *et al.*, "La-doped SnO2 as ETL for efficient planar-structure hybrid perovskite solar cells," *Org Electron*, vol. 73, pp. 62–68, Oct. 2019, doi: 10.1016/j.orgel.2019.03.053.

[80] D. Rehani, M. Saxena, P. R. Solanki, and S. N. Sharma, "Transition Metal and Rare-Earth Metal Doping in SnO2 Nanoparticles," *J Supercond Nov Magn*, vol. 35, no. 9, pp. 2573–2581, Sep. 2022, doi: 10.1007/S10948-022-06283-9/METRICS.

Chapter 03
Introduction to Deposition and Characterization Techniques

This chapter underlines an introduction of the thin film deposition and characterization techniques used to study optoelectronic properties of the ETL and perovskite films. Further, it also describes the working principle of these techniques.

3.1 Deposition Process

3.1.1 Spin coating

Spin coating (SC) is a low-cost wet thin film coating technique which utilizes liquid-based solution precursors and disperse them uniformly on the substrates to obtain wet thin films. Usually, SC is used to achieve very thin film thickness usually in the regime of nanoscale [1]. Moreover, the easy processing and competitive cost make this technique more feasible research and laboratory scale level.

The Spin Coating working mechanism is classified into four steps, i.e., i) Deposition ii) Spin up, iii) Spin off and iv) Evaporation. In step-I, the precursors are dropped onto the flat substrate at low spin speed to disperse solution precursors under the influence of the centrifugal force. In step-II, the spin speed is raised to the desired spinning speed.

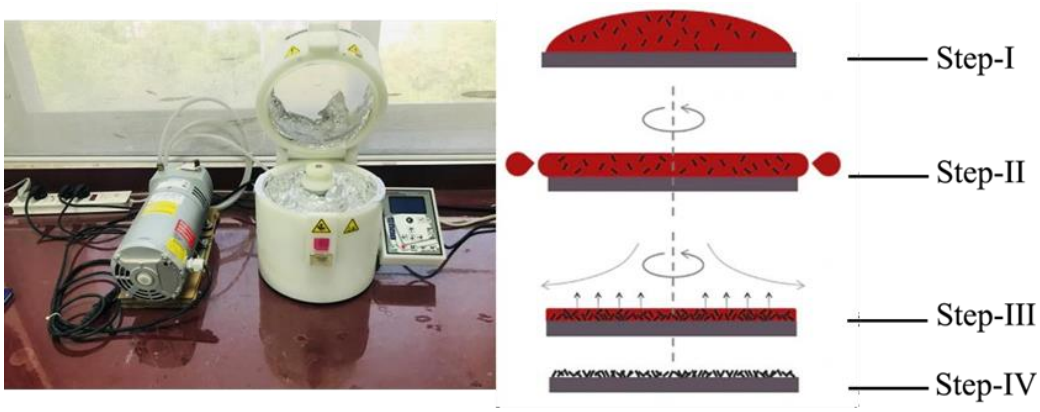

Figure 3.1. Image of spin coater instrument and schematic diagram of working mechanism

At this stage, the precursor or fluid on the substrate may be spinning at a different speed than the substrate itself. Then, in step-III, the extra fluid swung off from the substrate and

the wet film start changing its color indicating that the drying process of the thin film has started. Finally, in step-IV, the fluid speed and the substrate speech are matched which results in the thinning of the film because of the evaporation of the solvent as shown in Figure 3.1[2]. Spinning speed and ramping rate of the SC process play significant role to modulate thickness of the film.

3.1.2 Glove Box

Gloveboxes or commonly known as laboratory gloveboxes are mainly used to store ambient environment sensitive materials or perform sensitive fabrication processes which are difficult to be carried out in normal conditions. Actually, these devices create a closed environment which primarily a sealed and stable environment to protect sensitive material that can react with the air [3]. Normally, an artificial inert environment is created in gloveboxes using nitrogen or argon as an inert gas.

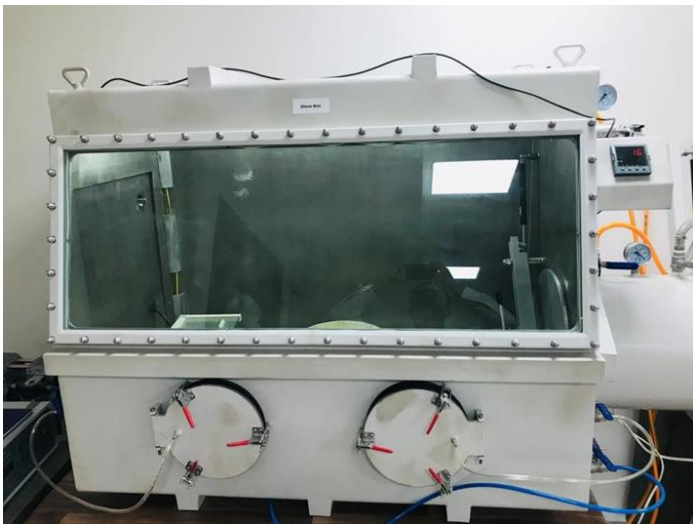

Figure 3.2. Image of humidity-controlled glovebox

A glovebox system consists of moisture (water) and oxygen sensors which show the levels of inside the glovebox. Moreover, it also comprises a heavy vacuum pump which is used to evacuate the glovebox chambers and to create an inert environment by purging nitrogen or argon gas.

3.1.3 Plasma Cleaning

Plasma cleaning is a surface cleaning process which is used to remove very small organic/inorganic particles, oil etc. from the surface of the substrate just prior to the

deposition of thin films. Normally substrates surfaces contain dust particles or organic residues which make these surfaces hydrophobic making it difficult to spin coat solution processable thin films. As a results, these surfaces are not covered completely during the deposition process. To counter this, a cleaning technique, known as plasma cleaning, is used to make the substrate surface more hydrophilic for the deposition of the thin films.

Glass substrates, fluorine doped tin oxide (FTO) or indium doped tin oxide (ITO), are placed inside the plasma cleaner to remove small residual particles from the glass substrate surfaces. Then, the chamber is closed, and vacuum pump is turned on to completely evacuate the air present inside to create a vacuum. Afterwards, a mixture of oxygen and argon is injected inside the chamber to create a purple color plasma for the removal of any contamination present on the surface of the ITO glass substrates. Normally, 10-20 minutes of the plasma treatment is suggested before the deposition of the thin films.

Figure 3.3. Image of plasma cleaner instrument

3.2 Characterization Techniques

3.2.1 UV-Vis-NIR Spectroscopy

UV-Vis-NIR spectroscopy is an analytical tool which is used to study light spectrum response (absorbance, transmittance, and reflectance) of liquids and solid samples. It has been frequently used to probe materials such as semiconductors, thin film coatings, glass etc. UV-Vis-NIR spectroscopy works on the principal of the Beer Lambart's law which

states that the absorbance of a solution directly proportional to the concentration of the absorbing material present in the solution [4].

Beer Lambart's law is stated by the following equation:

$$A = log\frac{I_o}{I} = \varepsilon lc = \alpha l \qquad \text{Eq (1)}$$

Where 'A' represents optical density or absorbance, Io represents the incident light intensity, and 'I' represents transmitted light intensity, the molar extinction coefficient, 'ε', the concentration of a solution sample, 'c', and the absorption coefficient 'α'. Moreover, the fraction $\frac{I_o}{I}$ also represents transmittance.

Generally, UV-Vis-NIR spectrophotometers are of two types known as single beam and double beam-based spectrophotometers. Single beam UV-Vis-NIR spectrophotometers are divided into four major components as shown in Figure 3.4.

- Light source
- Monochromator
- Sample
- Detector

A continuous light beam is generated by light source enters into the monochromator chamber. Where the continuous light spectrum is split into discrete photons based on different wavelengths. Afterwards, the monochromatic light is directed on the sample where it is either absorbed, transmitted, or reflected back. Then, the response of the sample after interacting with the light beam is recorded by the designated detectors against the different wavelengths [5].

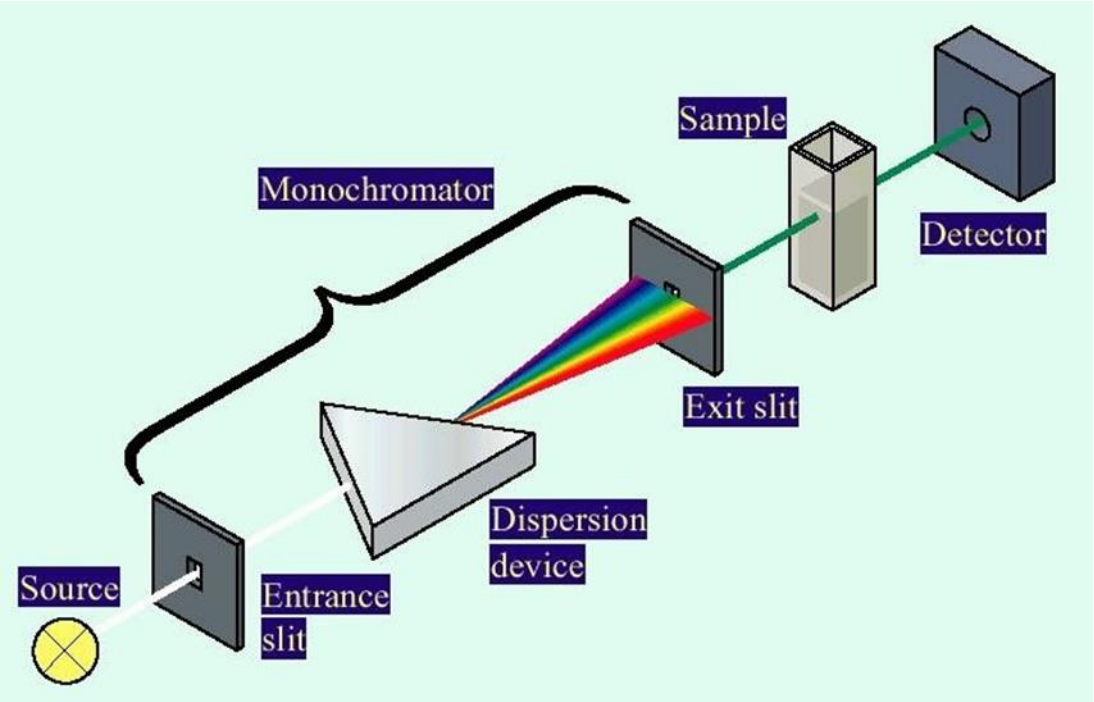

Figure 3.4. Schematic diagram of UV-Vis-NIR spectrophotometer working mechanism [5]

3.2.2 X-Ray Diffraction (XRD)

X-Ray diffraction or XRD is a non-destructive analytical technique which is used to study the structural and crystallographic properties of the powdered and thin film-based samples. It is also used to analyze crystal structure crystallinity of the samples. Moreover, it can also be used to identify the sample's crystalline phases, concentration profiles, film thickness and atomic patterns.

In XRD, the collimated beam of X-rays that has wavelength in the range $\lambda \sim 0.5\text{-}2$ Å is objected on a sample and then diffracted by the different crystalline phases as per relation the $\lambda = 2d\sin\theta$ (Bragg's law) where d is the interatomic spacing in the crystalline phase [6]. XRD diffractometers are composed of three main units:

- X-Ray tube
- Sample mounting stage
- X-Ray detector

X-Rays are generated inside the X-Ray tubes where an electron beam is produced by heating a filament. Then these electrons are accelerated by applying voltage and

bombarded on a target material. Afterwards, the electron beam that has sufficient energy dislodge the inner shell electrons of the target and as a result characteristic X-Rays are produced. Then these X-Rays are directed on the specimen at an angle of θ. Whereas an X-Ray detector is placed at angle of 2θ to record the diffracted X-Rays. The geometry of the diffractometer is such that the sample mounting stage is continuously rotating in the path of the collimated X-Ray beam. The instrument maintaining the angle and rotating the sample mounting stage is usually known as goniometer [7].

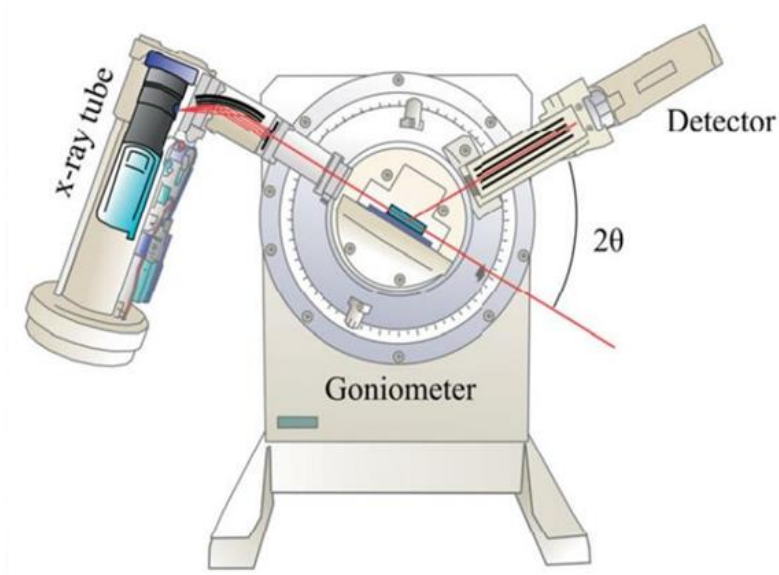

Figure 3.5. Schematic diagram of working mechanism of X-Ray Diffractometer [8]

3.2.3 Scanning Electron Microscopy (SEM)

A scanning electron microscopy is a non-destructive imaging technique used to analyze or record an image of a specimen under observation. It provides information about the sample surface texture, morphology, and chemical composition. It has been frequently used to study solid powder or thin films-based specimens.

In the SEM, a focused electron beam is bombarded on to the specimen and raster scanned over a small rectangular area. When the focused beam of electrons interacts with specimen's surface, various types of phenomena (emission of secondary electrons, photon emissions etc.) take place. This response can be efficiently recorded on a detector which ultimately forms an image based on the brightness of these electrons on traditionally used cathode ray tube. These images are just like the optical microscope images but with higher

magnification with a depth of a nanoscale regime [9]. Generally, SEMs consist of the following components:

- Electron source gun
- Electron lenses
- Sample mounting stage
- Detectors, for all types of electrons or signals
- Display or output systems

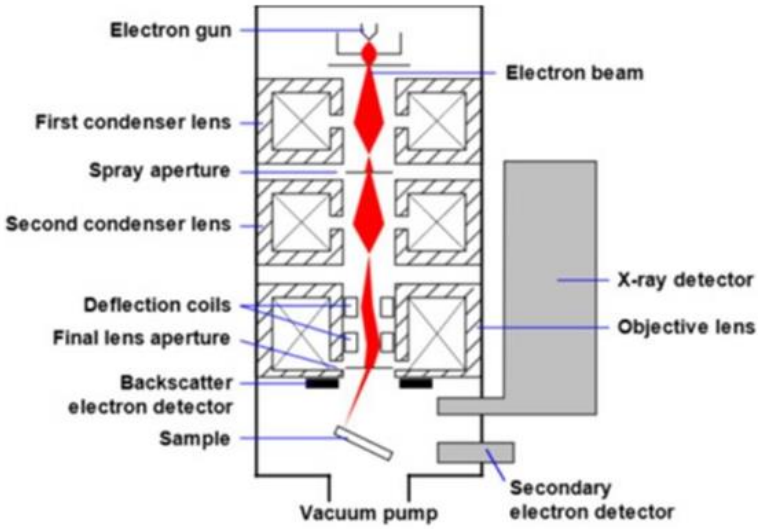

Figure 3.6. Working mechanism of SEM [10]

3.2.4 Hall Effect Measurement System

The Hall effect is used for the measurement of the electrical properties of a thin film. It gives information about charge carrier concentration, sheet resistance, resistivity, and the conductivity of the deposited thin film. It is recommended to prepare hall effect samples on simple glass slides to get an accurate estimate. Charge carriers participating in the flow of current are estimated by this characterization technique.

The hall effect measurement system consists of a magnet, sensing circuit, and a sample placement holder respectively. The sample is placed in the holder with 4 pins that serve as contact points on the thin films. A defined amount of current is passed from the points and the magnetic field is applied through the magnet. Hall voltage is measured corresponding to the applied current and the magnetic field as shown in Figure 3.7.

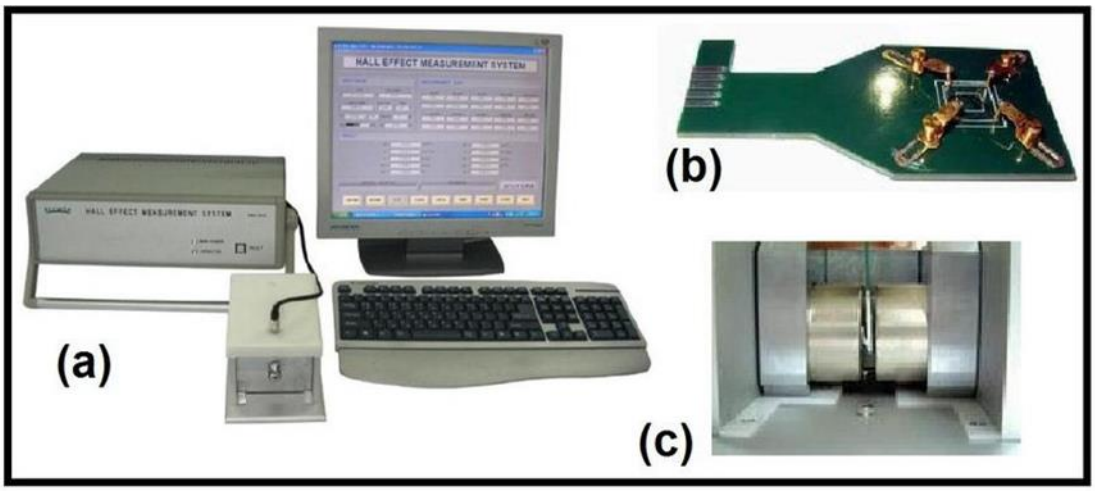

Figure 3.7. Hall Effect Measurement System [11]

The measure of the hall voltage at the point when a balance between the energy of electrons due to an electric and magnetic field is achieved is called the magnetic flux. The relation between the hall voltage and magnetic flux, in turn, gives information about all the other electrical parameters. Special software is used for these calculations that are often incorporated with the system [12]. Very small changes up to mA can be sensed with a hall effect system. Sample dimensions are very important for the accurate measurement of the deposited films. Samples should be prepared in equal square dimensions to collect the correct estimates of charge carriers present in the film.

3.2.5 Contact Angle Measurement System

Contact angle measurement is an analysis technique to analyze the hydrophobic/hydrophilic behavior of a thin film. It can also give estimates about the roughness of a film by analyzing the behavior of solutions on the surface when they meet the solid layer. This instrument measure the angle of contact between solid and liquid phases. Contact angle greater than 90° means the deposited film shows a hydrophobic behavior [13].

The sample is placed on a moveable stage and a water drop of a predefined size in microliters is dropped on the surface of the substrate. A light source illuminates the sample and the applied droplet. A 60-fps camera placed on the opposite side records a predefined time-stamped video [14]. The brightness of the image can also be manually controlled by a manual dial on the equipment as shown in Figure 3.8.

Built-in software tools are then used to trace the boundaries of the droplet and the contact angle is calculated automatically.

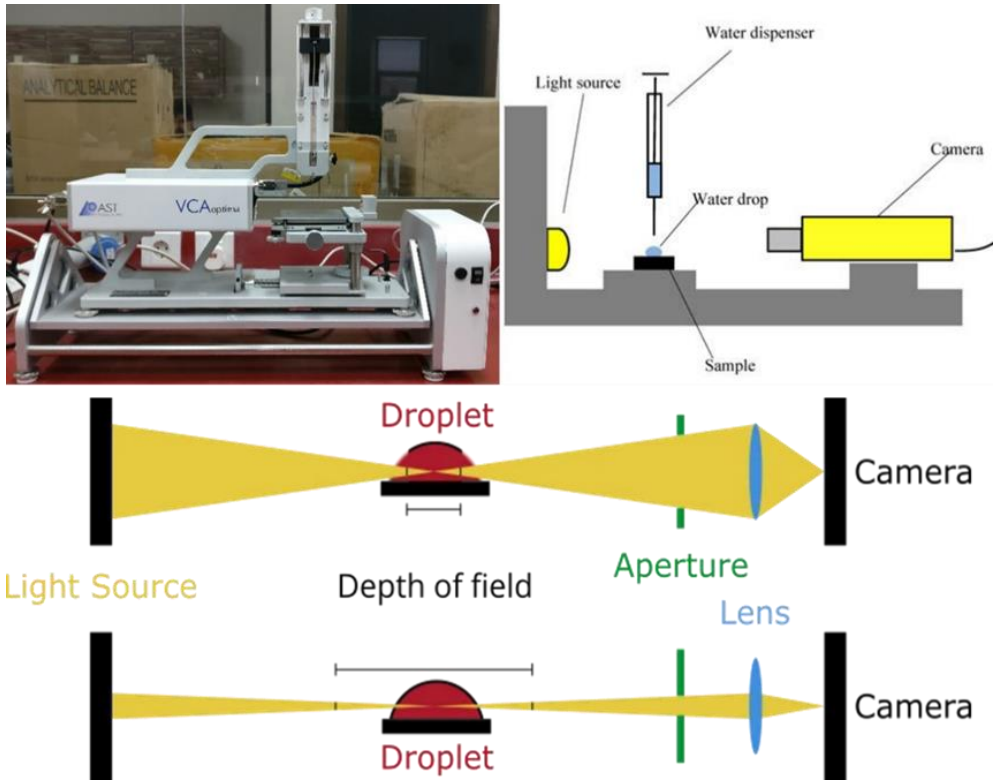

Figure 3.8. Contact angle measurement system working principle schematic [15].

3.2.6 Photoluminescence (PL) Spectroscopy

Photoluminescence spectroscopy also known as PL is a non-contact method of analyzing materials by the interaction of light. It gives information related to bandgaps, recombination mechanisms, molecular structures, impurity and defect detection, and crystallinity. Samples can be used in the form of powder, film, or liquid [16].

It works when the light energy energizes a material to emit a photon. The light is made to fall on the subject material, and it gets absorbed causing photoexcitation in the material. The absorption of a high-energy beam of light causes a jump in the electronic state and a photon (energy) is released when it returns to the lower energy level.

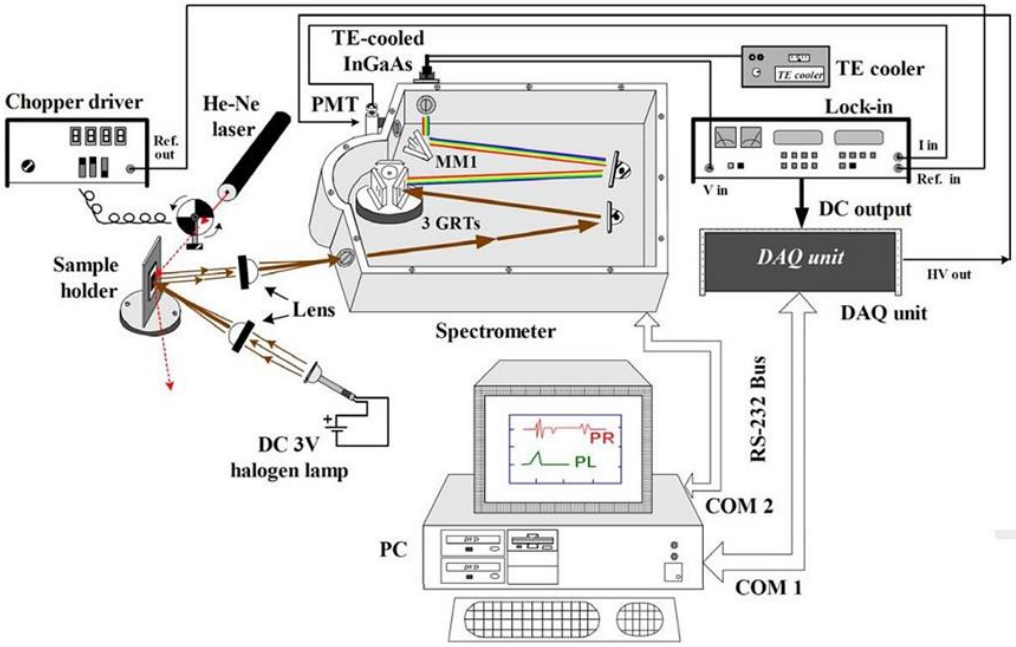

Figure 3.9. Working principle of photoluminescence spectroscopy [17].

This emission of photon or light is called luminescence hence the process of photoluminescence. The recorded emission peaks are further analyzed in built-in software.

Summary

This chapter introduces various thin film deposition and characterization techniques for studying opto-electronic properties of ETL and perovskite films, including spin coating, glove boxes, plasma cleaning, UV-Vis-NIR spectroscopy, X-Ray Diffraction (XRD), Scanning Electron Microscopy (SEM), Hall Effect Measurement System, Contact Angle Measurement System, and Photoluminescence Spectroscopy (PL). These techniques are essential for creating uniform nanoscale films, protecting and handling sensitive materials, cleaning substrate surfaces, analyzing light spectrum response, determining structural and crystallographic properties, imaging specimens, measuring electrical properties, analyzing hydrophobic/hydrophilic behavior, and examining material interactions with light.

References

[1] A. G. Emslie, F. T. Bonner, and L. G. Peck, "Flow of a viscous liquid on a rotating disk," *J. Appl. Phys.*, vol. 29, no. 5, pp. 858–862, 1958, doi: 10.1063/1.1723300.

[2] "Spin Coating: Complete Guide to Theory and Techniques | Ossila." https://www.ossila.com/pages/spin-coating (accessed May 10, 2023).

[3] "Glove Box Design | Ossila." https://www.ossila.com/pages/glove-box-application-notes (accessed May 10, 2023).

[4] "Beer-Lambert Law - an overview | ScienceDirect Topics." https://www.sciencedirect.com/topics/engineering/beer-lambert-law (accessed May 10, 2023).

[5] "UV-3600i Plus - Features : Shimadzu Scientific Instruments." https://www.ssi.shimadzu.com/products/uv-vis/uv-vis-nir-spectroscopy/uv-3600i-plus/features.html (accessed May 10, 2023).

[6] "X-ray diffraction | Definition, Diagram, Equation, & Facts | Britannica." https://www.britannica.com/science/X-ray-diffraction (accessed May 10, 2023).

[7] "X-ray Powder Diffraction (XRD)." https://serc.carleton.edu/msu_nanotech/methods/XRD.html (accessed May 10, 2023).

[8] "Scanning Electron Microscopy (SEM)." https://serc.carleton.edu/research_education/geochemsheets/techniques/SEM.html (accessed May 10, 2023).

[9] "Scanning Electron Microscopy - Nanoscience Instruments." https://www.nanoscience.com/techniques/scanning-electron-microscopy/ (accessed May 10, 2023).

[10] "Four Point Probes — Four-Point-Probes offers 4 point probe equipment for measuring the sheet resistance and bulk (volume) resistivity of materials used in the semiconductor industry, universities, and in materials science including thin films,

wafers, ingots, and other materials and conductive coatings." https://four-point-probes.com/ (accessed May 08, 2023).

[11] "Definition, Working Principle, Application & Examples of Hall Effect Sensor." https://www.elprocus.com/hall-effect-sensor-working-principle-and-applications/ (accessed May 08, 2023).

[12] M. Abe, "Contact Angle Measurement for Solid Surface," *Meas. Tech. Pract. Colloid Interface Phenom.*, pp. 129–135, 2019, doi: 10.1007/978-981-13-5931-6_18.

[13] "Contact Angle Measurement, Theory & Relation to Surface Energy | Ossila." https://www.ossila.com/pages/contact-angle-theory-measurement (accessed May 08, 2023).

[14] D. Szyszka and W. Szczepanski, "Contact angle of copper-bearing shales using the sessile drop and captive bubble methods in the presence of selected frothers," *Min. Sci.*, vol. 22, pp. 191–199, 2015, doi: 10.5277/msc152216.

[15] A. Gao, P. J. Rizo, L. Scaccabarozzi, C. J. Lee, V. Banine, and F. Bijkerk, "Photoluminescence-based detection of particle contamination on extreme ultraviolet reticles," *Rev. Sci. Instrum.*, vol. 86, no. 6, 2015, doi: 10.1063/1.4922883.

[16] "Photoluminescence and Photoreflectance - HORIBA." https://www.horiba.com/int/scientific/applications/energy/pages/photoluminescence-and-photoreflectance/ (accessed May 08, 2023).

Chapter 04
Experimental Work

This chapter illustrates the experimental work performed to prepare the electron transport layer precursors, substrate preparation and the fabrication of the perovskite films. In addition, it also describes the parameters used to characterize these films.

4.1 Materials

Tin (II) Chloride Dihydrate (CAS No. 10025-69-1), La (III) Chloride Heptahydrate (CAS No. 10025-84-0) Methylammonium Iodide (CAS No. 14965-49-2), Lead (II) Iodide (CAS No. 10101-63-0), Cesium Bromide (CAS No. 7787-69-1), N, N Dimethylformamide (CAS No. 68–12-2), Dimethyl sulfoxide (CAS No. 67–68-5) and Florine-doped Tin Oxide (FTO) glass substrate (EC No. 242-159-0) were sourced from Sigma-Aldrich. All of these materials were used exactly as they were received, with no extra purification steps.

4.2 Preparation Method of Electron Transport Layers

0.1mol/L solution of $SnO_2.2H_2O$ in absolute ethanol was prepared through refluxing at 80° C for 3 hours. The solution was then aged for about 1 week. For lanthanide doping precursor, 0.1mol/L solution of $LaCl_3.7H_2O$ in absolute ethanol was prepared. To prepare volume ratio La (III) doped solutions, 10µL, 20µL, 30µL of the La (III) doping precursor was added into 490µL, 480µL, 470µL of SnO_2 precursor, yielding 2%, 4%, and 6% La: SnO_2 solutions respectively. The precursor solutions were filtered through 0.22µm PTFE filters before use. The FTO substrates were cleaned through sonication in deionized water, 2-propanol, acetone, and 2-propanol sequentially for 15 mins each. After sonication, the substrates were dried with nitrogen gun and plasma cleaned for 10 mins. The precursors were spin coated onto clean FTO for 30s at 2000 rpm and then annealed at 250° C for 3 hours.

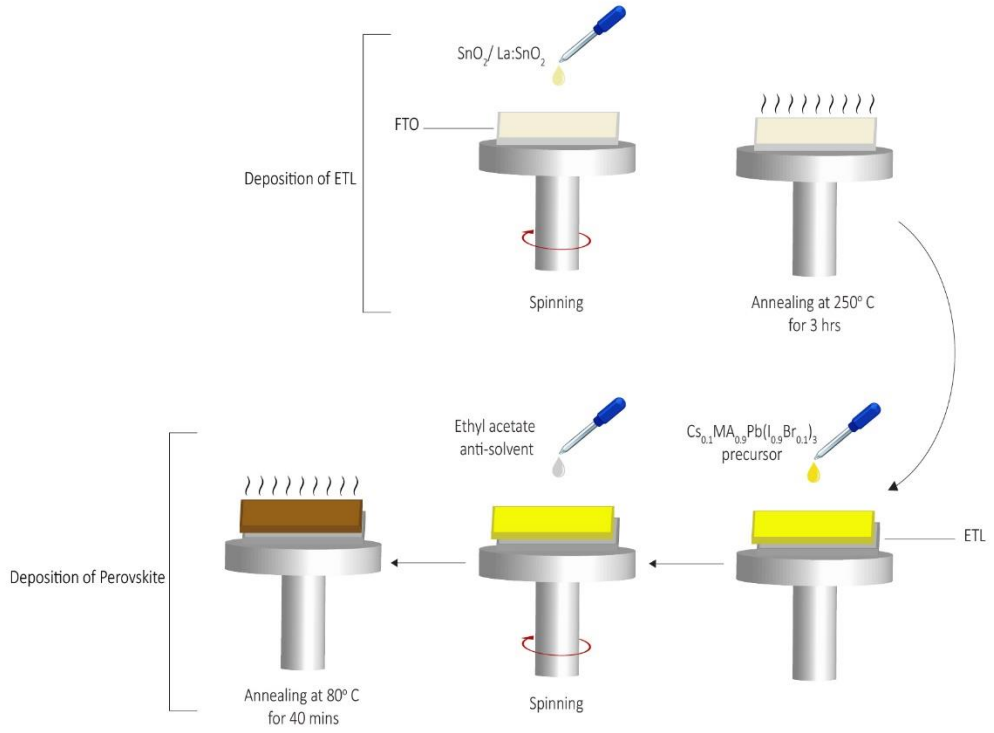

Figure 4.1. Schematic illustration of the deposition of ETL and perovskite layer on FTO glass substrate

4.3 Preparation Method for Perovskite Layer

$Cs_{0.1}MA_{0.9}Pb(I_{0.9}Br_{0.1})_3$ precursor mixture was formulated by combining 461 mg of lead iodide, 143 mg of methylammonium iodide, and 21 mg of cesium bromide in 1 ml of a solvent composed of DMF and DMSO with a 4:1 volume proportion. The blend was stirred at 70°C for a 12-hour period and then passed through a 0.22 µm PTFE filter. The resulting liquid was applied to the ETLs using a two-step spin coating, initially at 500 rpm for 3 seconds and then at 4000 rpm for 30 seconds. In the last 10 seconds of rotation, ethyl acetate was introduced as an antisolvent. Finally, the spin coated film was annealed at 80°C for 40 minutes under standard atmospheric conditions. Figure 4.1 shows the sequential deposition of ETL and perovskite layer onto FTO substrate.

4.4 Film Characterizations

A range of characterization methods have been utilized to examine the film's structure and morphology, its composition, as well as its hydrophobic and hydrophilic traits, in addition to its optoelectronic properties.

4.4.1 X-Ray Diffraction (XRD)

The structural characteristics and crystallite sizes of the films were investigated using X-ray Diffraction (XRD) analysis on a Bruker D8 Advanced instrument, with a scan rate of 1.25°/min and a 2θ range from 10° to 80°. Cu Kα radiation (λ = 1.542 Å) was employed with a 40 kV activation voltage and a 30-mA current. MDI's Jade 6.5 software was utilized for peak assessment and signal processing.

4.4.2 Scanning Electron Microscopy (SEM)

A Scanning Electron Microscope (SEM, JEOL Japan) was employed to study morphology of the films, with images captured at a 20.0 kV voltage.

4.4.3 UV-Vis-NIR Spectroscopy

ETL and perovskite films' optical properties were analyzed using a UV-3600 Plus Ultraviolet-Visible NIR Spectrophotometer with a 2.5 µm slit width. Measurements of transmittance and absorbance were conducted in the 250–1100 nm wavelength range.

4.4.4 Hall Effect Measurement

The ECOPIA HMS-3000, a sophisticated and versatile instrument, was employed to carry out Hall effect measurements in order to comprehensively assess the electrical properties of the electron transport layers.

4.4.5 Contact Angle Measurement

A VCA Optima device from ASTP was used for contact angle analysis under standard atmospheric conditions, using a 30 µL droplet of de-ionized water.

4.4.6 Photoluminescence (PL) Analysis

A steady-state photoluminescence (PL) spectra were obtained with a Horiba Scientific iHR320 spectrophotometer, employing an excitation wavelength of 450 nm.

Flow Chart

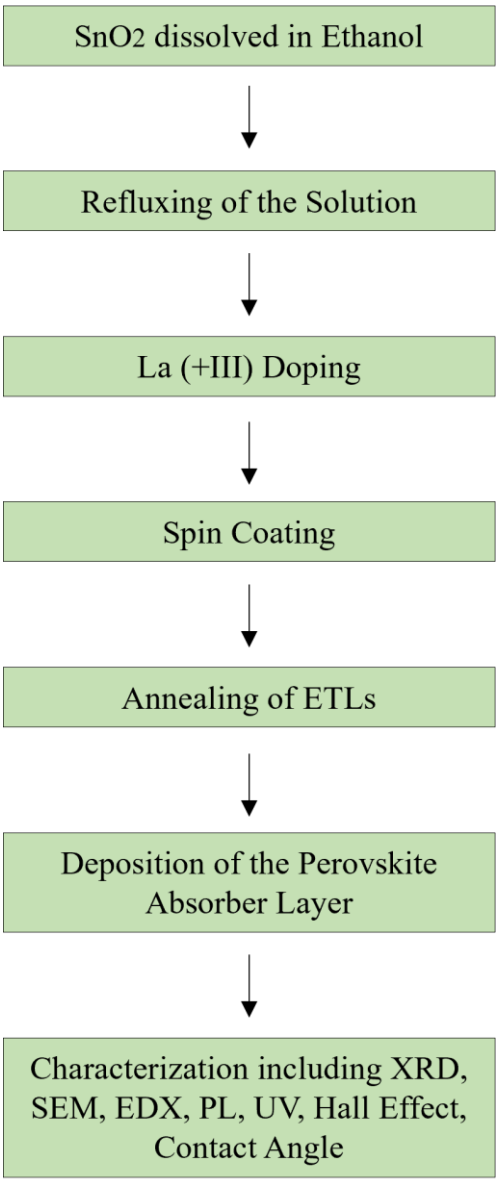
SnO2 dissolved in Ethanol
Refluxing of the Solution
La (+III) Doping
Spin Coating
Annealing of ETLs
Deposition of the Perovskite Absorber Layer
Characterization including XRD, SEM, EDX, PL, UV, Hall Effect, Contact Angle

Summary

This chapter details the experimental work conducted to prepare electron transport layer precursors, substrate preparation, and the fabrication of perovskite films. The materials used were sourced from Sigma-Aldrich and did not require additional purification. The chapter outlines the preparation methods for the electron transport layers, with various lanthanide doping levels, and the perovskite layer. The fabrication process involved spin coating and annealing.

The films were characterized using a variety of techniques, including X-Ray Diffraction (XRD) to study structural characteristics, Scanning Electron Microscopy (SEM) for morphology analysis, UV-Vis-NIR Spectroscopy for optical properties assessment, Hall Effect Measurement for electrical properties evaluation, Contact Angle Measurement to determine hydrophobic and hydrophilic properties, and Photoluminescence (PL) Analysis to examine the films' light-emitting properties.

Chapter 5
Results and Discussions

The chapter on results and discussion sheds light on the study's findings and explains their importance in the context of the research objectives. Through the assessment of data procured from a range of characterization techniques, the diverse surface, structural, electrical, and optical attributes of the pure and doped electron transport thin films are thoroughly explored and discussed.

5.1 Structural Analysis

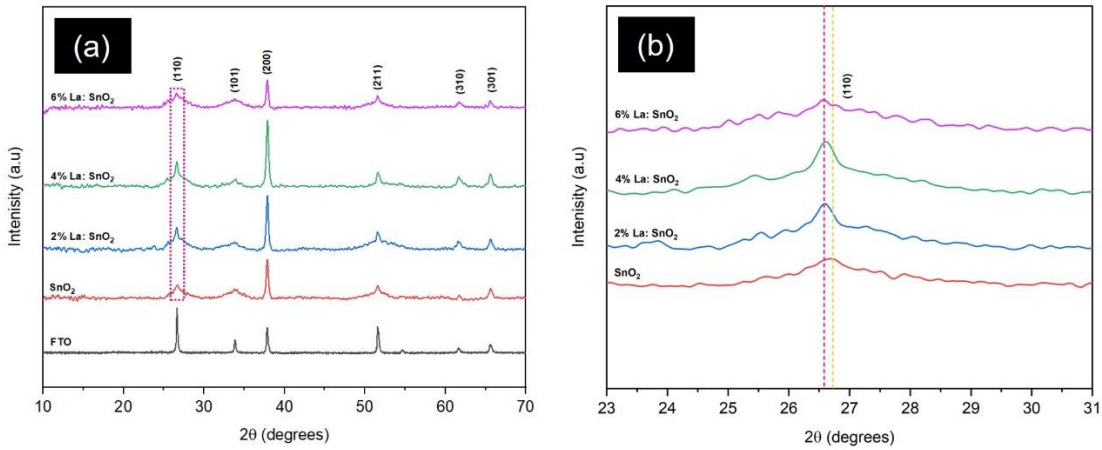

Figure 5.1. XRD spectra of the (a) FTO, SnO_2, and doped ETLs (b) The shift in the plane (110)

The XRD patterns of pure SnO_2 and La-doped (2%, 4%, 6%) SnO_2 films, grown on FTO, were analyzed to gain insights into their crystal structure. Thin films were annealed at 250°C for 3 hours in an ambient environment. The results demonstrated that all the films displayed the rutile tetragonal structure of SnO_2, with the most intense planes in the (110) and (200) orientations at 2θ positions of 26.6° and 37.9°. Additionally, less intense diffraction peaks were observed at 2θ positions of 33.8°, 51.7°, 61.8°, and 65.9°, corresponding to the hkl planes (101), (211), (310), and (301), respectively. These findings aligned with JCPDS-card no. 41-1445, associated with the space group P42/mnm. The absence of other secondary phases in the XRD pattern confirms that La(III) ions have been successfully incorporated into the SnO_2 crystal lattice without disrupting the rutile

tetragonal lattice. Similar findings have been reported by Bouznit et al. [1], Sivakumar et al. [2], and Gao et al. [3].

The intensity of all the diffraction planes increased upon doping, suggesting improved SnO_2 crystallinity due to the addition of trivalent La(III) impurity. Figure 5.1 b. demonstrates a slight shift for the (110) plane towards a lower angle as the doping concentration rises to 6%. This shift verifies the integration of La(III) ions into the tetragonal crystal lattice of SnO_2 [1]. The shift in the plane can be ascribed to the growth of the crystal lattice and increased interplanar spacing in the lattice because of the difference in the ionic radii of parent ions Sn(IV) (0.69 Å) [4] and dopant ions La(III) (1.03 Å) [5]. The variation in d-spacing values; as tabulated in Table 4; results from the relatively larger size of La(III) ions compared to Sn(IV) ions, confirming the successful incorporation of La(III) into the SnO_2 lattice [1], [4], [6].

Table 4. Multiple parameters for pristine and La-doped SnO_2

Composition	(hkl)	FWHM (β)	Center (2θ)	Height	Crystallite Size (D) (nm)	d Spacing (Å)	Dislocation density (δ) $X10^{-3}$ lines/m^2	% Micro strain (ε)
SnO_2	110	1.68	26.67	114.65	5.06	3.339	39.00	43.34
2% La: SnO_2	110	1.21	26.59	181.38	7.03	3.349	20.25	33.90
4% La: SnO_2	110	0.76	26.61	196.32	11.20	3.346	7.98	20.84
6% La: SnO_2	110	2.73	26.57	148.90	3.13	3.351	102.33	77.78

In the present study, the average crystallite size (D) values corresponding to the primary peak of the (110) plane were measured for ETLs deposited on FTO substrates using the well-established Debye-Scherrer formula [7], The corresponding results are presented in Table 4.

$$D = \frac{0.9\lambda}{\beta cos\theta} \qquad \text{Eq (2)}$$

Here, D, λ, β, and θ represent the average crystallite size, the wavelength of X-rays, the full width at half maximum (FWHM) in radians, and Bragg's angle, respectively. As indicated in Table 4 and Figure 5.2 a, the FWHM (β) for the (110) plane achieves its minimum value at 4% La doping, resulting in the largest crystallite size of 11.2 nm. When La content is increased beyond 4%, the crystallite size decreases to its minimum value. At

6% La: SnO_2, peak broadening occurs, the FWHM increases, and the overall crystallite size of the film is reduced.

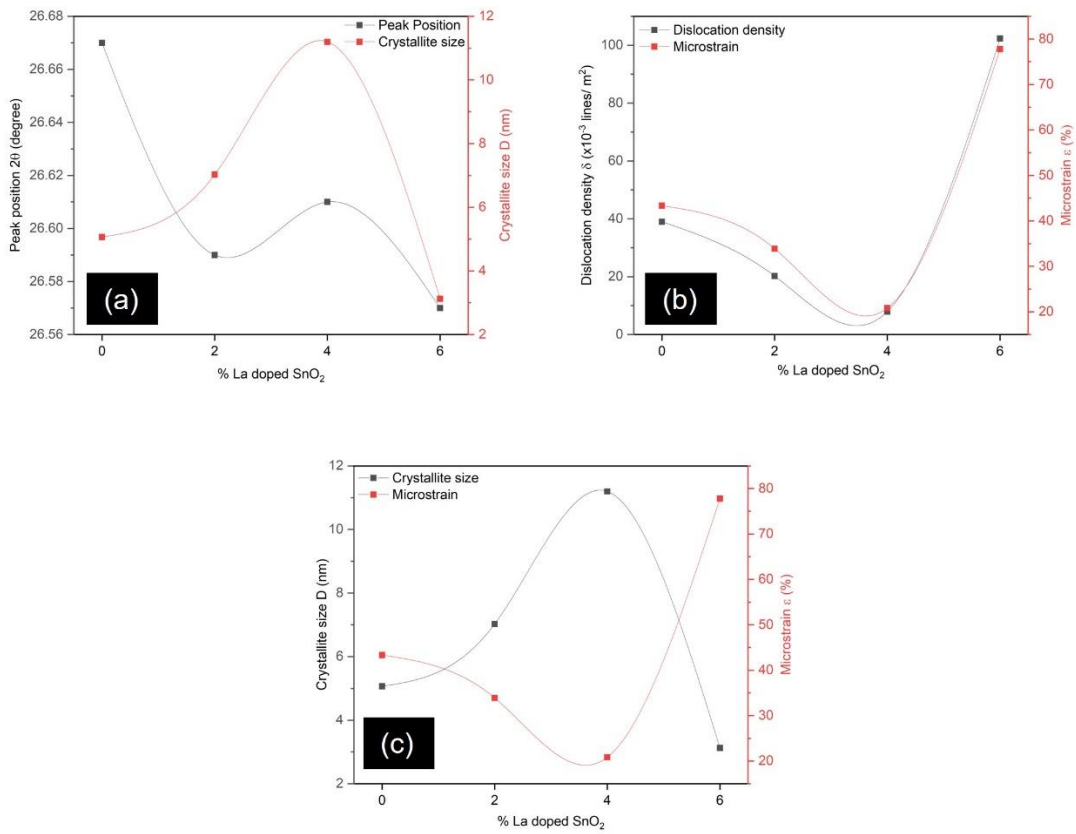

Figure 5.2. Trend of parameters of the (110) plane mentioned in Table 1 (a) Peak Position vs Crystallite Size, (b) Dislocation density vs Microstrain, (c) Crystallite size vs Microstrain

Furthermore, the dislocation density (δ) and percent microstrain (ε) for the (110) plane was determined using the following equations [8].

$$\delta = \frac{1}{D^2} \qquad \text{Eq (3)}$$

$$\varepsilon = \frac{\beta \tan \theta}{4} \qquad \text{Eq (4)}$$

The calculated values for the dislocation density and microstrain are provided in Table 4 and presented in Figure 5.2. It is observed from Figure 5.2 b. that the dislocation density ($x10^{-3}$ lines/m^2) in the SnO_2 lattice (39.0) is significantly reduced to (7.98) upon incorporating up to 4% La into the crystal lattice. However, the dislocation density, and

hence the crystal imperfections increase once again as the dopant concentration exceeds 4%. The microstrain follows a similar trend, increasing at 6% La: SnO_2. The rise in microstrain and dislocation density is ascribed to the difference in ionic radii between the parent tin (Sn) atom and dopant (La) atom, which induces substantial crystal imperfections as the dopant concentration surpasses 4%. Figure 5.2 c. demonstrates that the introduction of a La(III) into the SnO_2 lattice increases the crystallite size and reduces the microstrain values. However, doping beyond 4% leads to a decreased crystallite size and a rise in lattice strains following previously reported similar trend. The improved crystallinity and reduced crystal imperfections in ETL are crucial for the uniform morphology and growth of deposited PAL [3], [4].

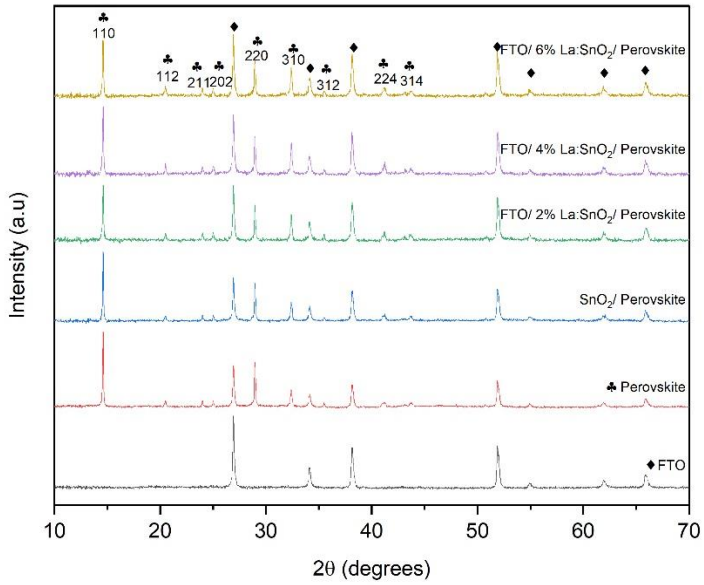

Figure 5.3. XRD spectra of $Cs_{0.1}MA_{0.9}Pb(I_{0.9}Br_{0.1})_3$ absorber layer deposited over pristine SnO_2 and La:SnO_2

To probe the role of ETLs in perovskite films growth, XRD patterns of perovskite films deposited on different ETLs were acquired. Figure 5.3. presents the XRD results for the highly crystalline $Cs_{0.1}MA_{0.9}Pb(I_{0.9}Br_{0.1})_3$ PAL deposited onto various ETL with different compositions. All XRD patterns display sharp and intense diffraction peaks, indicating high crystallinity, irrespective of the underlying ETL compositions. The sharp peaks observed at 14.5°, 28.8°, and 32.3° correspond to the (110), (220), and (310) planes of $Cs_{0.1}MA_{0.9}Pb(I_{0.9}Br_{0.1})_3$ respectively [9], [10]. The weaker peaks can be assigned to the (112), (211), (202), (312), (224), and (314) planes, signifying highly crystalline perovskite

phase formation [9]. The perovskite structure remains unchanged upon deposition over the ETL, likely due to the consistent ETL morphology [11]. Cs^+ helps in crystallization of perovskite at room temperature along with entirely dissolving and converting PbI_2 into perovskite phase, which is indicated by the absence of the (001) plane for PbI_2 at 12.6 [12].

5.2 Optical and Electrical Characteristics

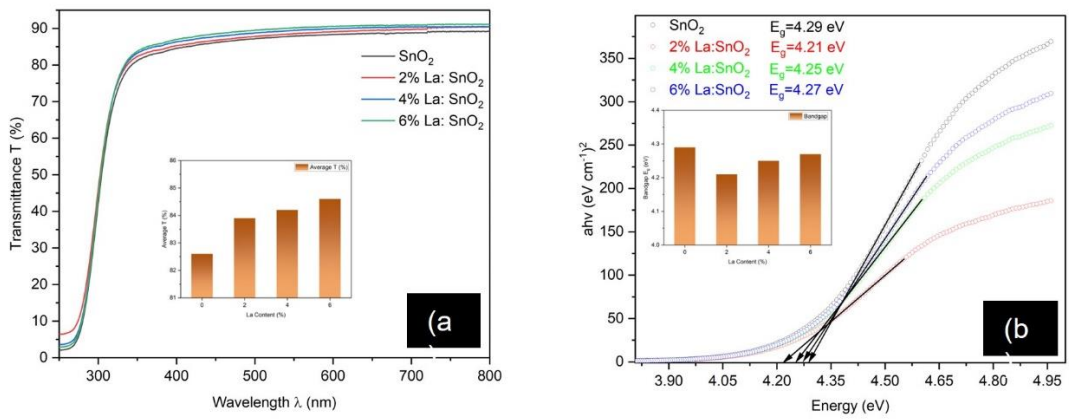

Figure 5.4. (a) Transmittance spectra of SnO_2 and La:SnO_2 ETLs, (b) Tauc plots for SnO_2 and La:SnO_2 ETLs

Figure 5.4 a. demonstrates the transmittance spectra of SnO_2 and La: SnO_2, in the visible region 380-700 nm. The spectra exhibit an increase in transmittance levels upon doping, with values calculated as 82.6%, 83.9%, 84.2%, and 84.6% for La doping concentrations of 0%, 2%, 4%, and 6%, respectively. This observation is in accordance with the findings reported by Zhou X et al. [4] and P. Sakthivel et al. [13], which stated that doped SnO_2 possess superior transmittance as compared to pristine and hence reduced parasitic light absorption at ETL. The optical bandgap values were measured using Tauc's plot among the absorption coefficient $(\alpha h\nu)^n$ (where n=2 for direct optical transition) and photon energy ($h\nu$), as shown in Figure 5.4 b. The bandgap values are 4.29 eV, 4.21 eV, 4.25 eV, and 4.27 eV for La doping concentrations of 0%, 2%, 4%, and 6%, respectively. An overall decrease in bandgap values was observed as dopant atoms were incorporated into the lattice [3], [14]. This is due to the reason that La doping reduced the bandwidth resulting in the downward shift of the fermi-level, confirming previously reported findings [3], [14], [15]. This results in an overall enhancement of charge extraction in doped ETLs and a

subsequently reduced recombination of charges at La:SnO_2/perovskite contact compared to the pristine SnO_2 [16].

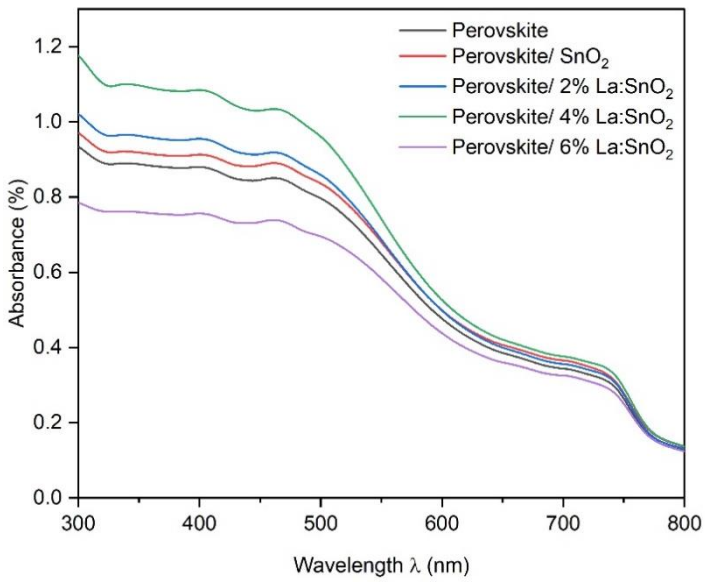

Figure 5.5. Absorbance spectra of $Cs_{0.1}MA_{0.9}Pb(I_{0.9}Br_{0.1})_3$ over SnO_2 and La:SnO_2 ETLs

The absorption characteristics of $Cs_{0.1}MA_{0.9}Pb(I_{0.9}Br_{0.1})_3$ absorber layer deposited on different substrates are presented in Figure 5.5. The results exhibited consistency with the transmittance spectra of the underlying ETLs. A notable enhancement in the light-harvesting properties of the perovskite is evident when deposited on all ETLs, including SnO_2, 2% La:SnO_2, and 4% La:SnO_2. We can attribute this higher absorption by perovskite layer to the improved transparency at ETLs and the development of a smooth absorber film with improved grain size over doped ETLs, as supported by SEM images [17]. Such enhanced absorption is crucial for superior device performance and higher current densities [18]. However, the absorption profile of perovskite deposited on 6% La:SnO_2 diminished, which is accredited to roughness of deposited perovskite film that results in more scattering of light [19].

Table 5. Electrical parameters of SnO_2 and La:SnO_2 ETLs

ETL Composition	Mobility ($cm^2 \cdot V^{-1} \cdot s^{-1}$)	Carrier Conc. ($x10^{21}$ cm^{-3})	Resistivity ($x10^{-5}$ $\Omega \cdot cm$)	Conductivity ($x10^4$ $\Omega \cdot cm)^{-1}$	Sheet Resistance ($\Omega \cdot cm^{-2}$)
SnO_2	1.22	4.12	5.96	1.67	1.19
2% La:SnO_2	1.94	5.74	5.58	1.78	1.11
4% La:SnO_2	2.53	9.51	5.36	1.86	1.07
6% La: SnO_2	1.49	7.31	5.72	1.74	1.14

Hall effect measurements of pure and La-doped ETLs, including conductivity, resistivity, sheet resistance, mobility, and carrier concentration are tabulated in Table 5. Pure SnO_2 samples display the highest resistivity and sheet resistance values while these parameters decrease substantially as the doping concentration increases up to 4% and increase again as the dopant amount reaches 6%. The higher values of resistivity and sheet resistance in SnO_2 and 6% La:SnO_2 are because of smaller crystallite sizes [20]. Moreover, mobility and carrier concentration follow the same trend. Whereas conductivity increases from $1.67x10^4$ $(\Omega \cdot cm)^{-1}$ to $1.86x10^4$ $(\Omega \cdot cm)^{-1}$ as it is inversely related to resistivity [21] and is maximum for 4% La:SnO_2. The recombinations at the interface of the SnO_2/ perovskite reduce significantly upon doping due to higher conductivity [16].

5.3 Morphology Study

The scanning electron microscopy (SEM) images depicted in Figure 5.6 (a-d). displays the surface morphology of ETLs deposited on FTO and Figure 5.6 (e-h). reveal the characteristics of $Cs_{0.1}MA_{0.9}Pb(I_{0.9}Br_{0.1})_3$ PAL spin-coated onto various underlying ETLs. Figure 5.6. shows that the smooth and densely packed ETLs entirely cover the FTO surface, thereby enhancing the quality of the perovskite layers grown on the ETLs' surface. The surface morphology of the SnO_2 ETL, grown on FTO Figure 5.6 a., reveals the formation of pinholes at the surface [22].

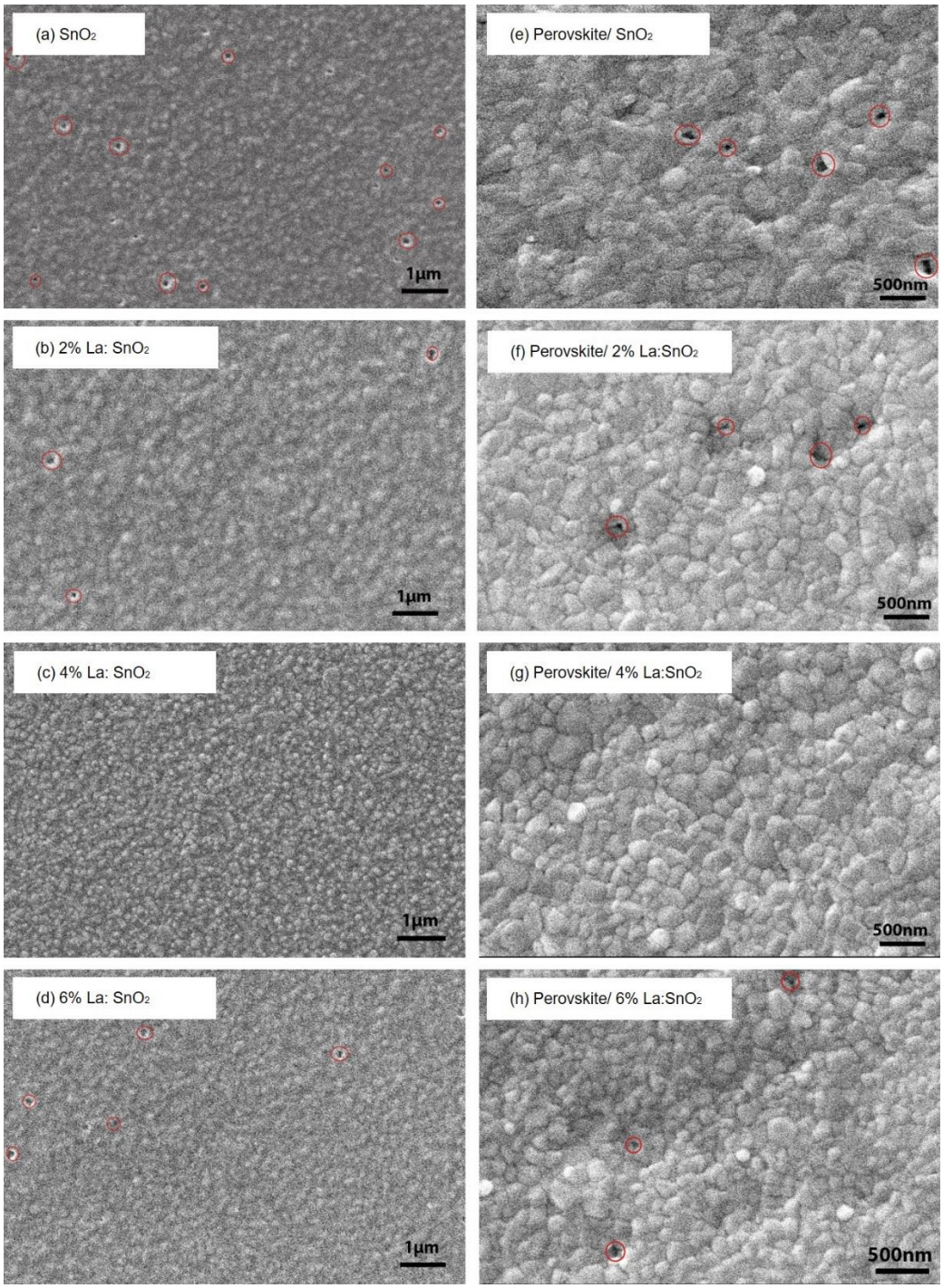

Figure 5.6. SEM images of (a-d) pristine and La-doped ETLs, (e-h) $Cs_{0.1}MA_{0.9}Pb(I_{0.9}Br_{0.1})_3$ deposited over different underlying ETLs

Pinholes serve as defect centers and recombination sites at the ETL-perovskite contact, and they severely impair device performance due to current leakages [23]. It is evident that the introduction of La(III) dopant into the lattice results in improved morphology and a significant reduction in pinhole formation for 2% La:SnO_2 (Figure 5.6 b.), as well as an

almost pinhole-free surface morphology for 4% La:SnO_2 ETL (Figure 5.6 c.). However, when the amount of dopant is raised from 4% to 6% (Figure 5.6 d.), the pinholes re-emerge on the surface, indicating the necessity for careful control and optimization of dopant quantity. It is evident that PAL grown over the SnO_2 (Figure 5.6 e.) exhibits small grain size with the presence of pinholes. The films display a smooth surface, and pinhole dimensions in the absorber layer deposited on highly crystalline 2% La:SnO_2 (Figure 5.6 f.) are reduced, nearly disappearing for PAL deposited on most crystalline 4% La:SnO_2 (Figure 5.6 g.). Upon depositing the absorber layer on 6% La:SnO_2 (Figure 5.6 h.), the re-emergence of pinholes and an increase in grain boundary density is observed, although pinholes' size is still smaller compared to those found in SnO_2. This poor surface morphology of perovskite deposited over 6% La:SnO_2 might be due to the poor interface that 6% La:SnO_2 provides, as illustrated in Figure 5.6 d. Therefore, optimized La(III) doping prevents structural and morphological defects present in SnO_2 that notably facilitates the increased grain size of PAL and minimize charge carrier recombinations.

5.4 Wettability Analysis

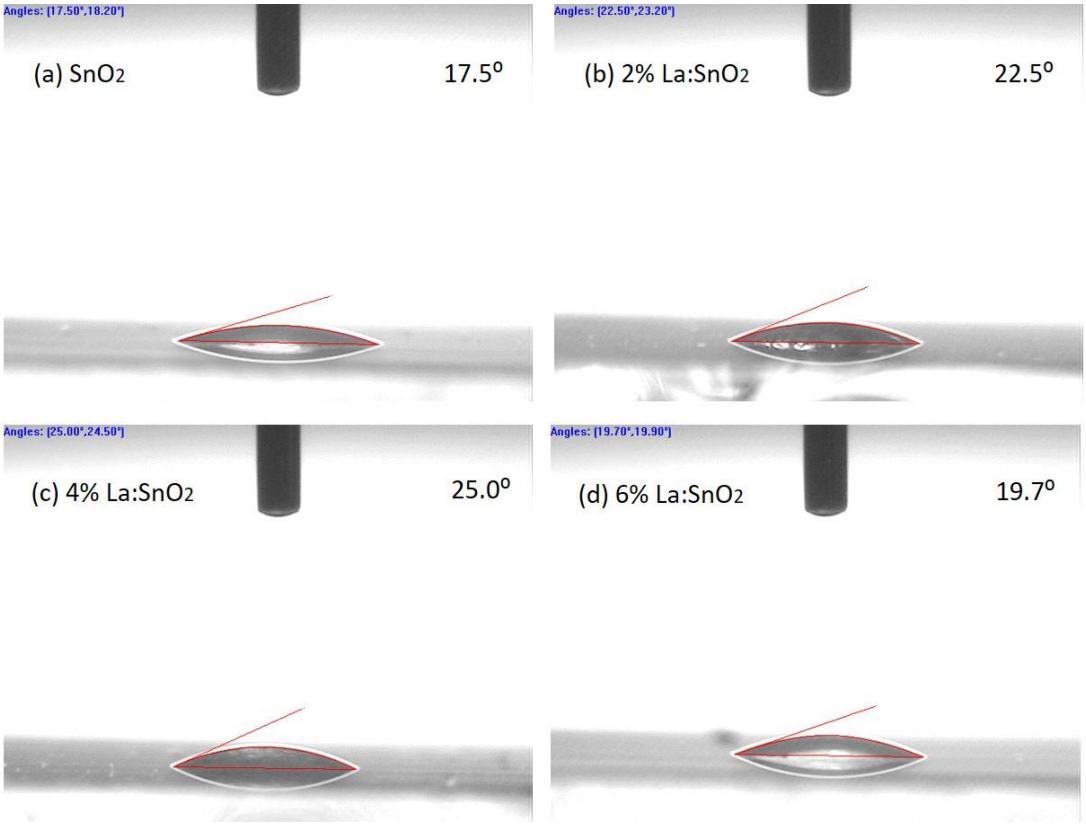

Figure 5.7. Wettability studies of SnO_2 and La:SnO_2 ETLs

Figure 5.7 (a-d). presents the wettability analysis of the pristine and La:SnO_2. Water contact angles were determined to be 17.5°, 22.5°, 25°, and 19.7° for SnO_2, 2%, 4%, and 6% La(III) doped ETLs, respectively. It is noteworthy that the contact angles for the 2%, 4%, and 6% doped samples are higher as compared to those of the pristine SnO_2. The increased contact angles for the ETL suggest a lower surface energy of the substrate, which is advantageous for reduced heterogeneous nucleation of the perovskite grown over ETL [24]. The less-dense nuclei of the perovskite contribute to uniform film coverage, larger grains, and reduced pinholes [24]. Upon raising the dopant concentration to 6% (Figure 5.7 d.), wettability is enhanced, and the contact angle decreases from 25° to 19.7°. The increased wettability of the 6% doped ETL substrate results in rapid crystallization of the absorber layer, owing to the small grains and formation of pinholes at the surface, as clear from SEM results (Figure 5.6 h.).

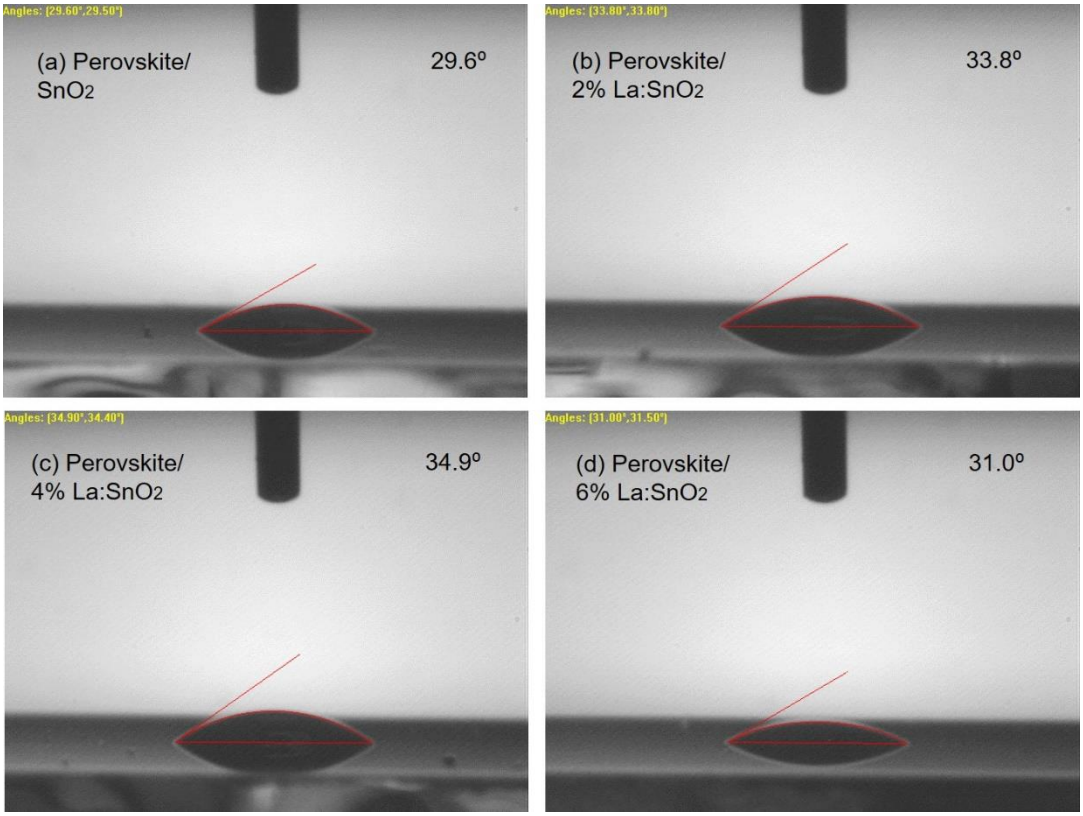

Figure 5.8. Wettability studies of perovskite deposited on SnO_2 and La:SnO_2 ETLs

The contact angle measurements in Figure 5.8. indicate the surface properties of perovskite films deposited on various ETLs. It is important to consider that grain boundary passivation changes surface wettability due to which the perovskite films deposited over

La:SnO_2 (Figure 5.8 b-d.) exhibit hydrophobic nature with higher contact angles [25]. Grain boundaries and pinholes present in perovskite films are a critical factor in initiating film degradation under moist conditions. Consequently, the passivation of these defects is advantageous for resisting the ingression of water molecules, reducing perovskite film decomposition, and enhancing device stability [26]. Films deposited on highly crystalline 2% and 4% La doped ETLs demonstrate relatively fewer grain boundaries, as evidenced by SEM images, resulting in most hydrophobic characteristics compared to films deposited on pure SnO_2 and 6% La:SnO_2. The hydrophobicity observed on the surface of PAL is also credited to the presence of Cs^+, which makes perovskite stable towards humidity and moisture [27].

5.5 Photoluminescence (PL) Studies

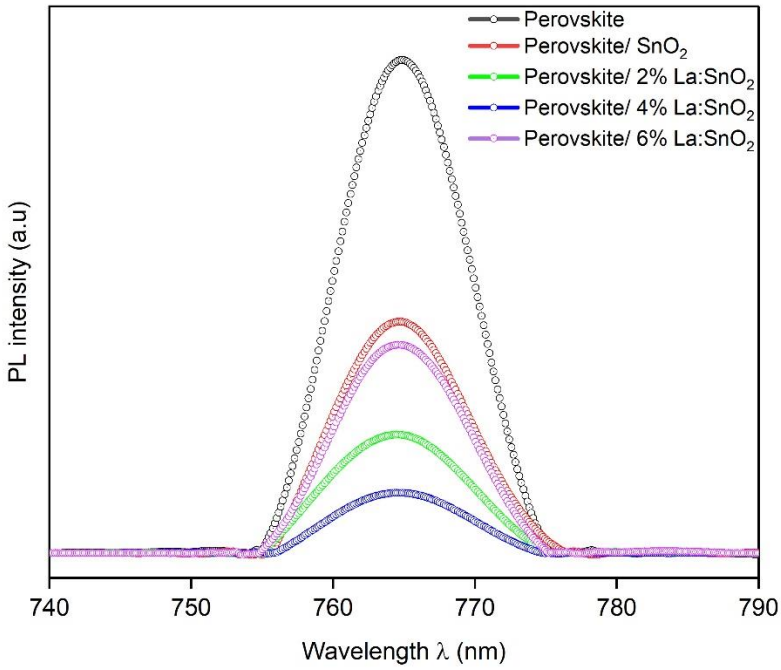

Figure 5.9. PL studies of Perovskite with SnO_2 and La:SnO_2 ETLs

To investigate the impact of La:SnO_2 on the recombination of carriers, the steady-state PL studies were conducted to probe the charge extraction kinetics at the Perovskite/SnO_2 and Perovskite/La:SnO_2 interfaces. Upon excitation at 450 nm, it is evident from Figure 5.9. that all samples, regardless of the underlying layer, exhibit a common peak at around 765 nm. The reduction in PL intensity corresponds to the extraction of carriers from the

perovskite layer into the ETL. The PL spectra reveals that the highest PL intensity is observed in perovskite without an ETL. In contrast, the introduction of pure SnO_2 and La:SnO_2 results in a substantial decrease in PL intensity, suggesting enhanced charge carrier injection and a decrease in defect density at the ETL-perovskite contact [13], [16], [28]. Notably, Perovskite/4% La:SnO_2 sample exhibits the most pronounced PL quenching, indicating that 4% La-doped SnO_2 serves as the most effective ETL for charge separation and transport, as supported by preceding results.

Summary

The chapter on results and discussion provides a comprehensive analysis of the structural, optical, electrical, and morphological properties of pure and La-doped SnO_2 electron transport thin films. Through X-ray diffraction (XRD), it is established that La doping enhances SnO_2 crystallinity without disrupting the rutile tetragonal lattice. Optimal doping concentration is found to be 4%, which leads to improved transmittance, reduced bandgap values, and enhanced conductivity. Scanning electron microscopy (SEM) images reveal that La doping improves the surface morphology and decreases pinhole formation in electron transport layers, resulting in better perovskite absorber layers. The study also examines the wettability and hydrophobic properties of perovskite films, with optimal results observed at 4% La doping concentration. Photoluminescence studies further confirm the enhanced charge extraction and reduced recombination at the optimal doping concentration.

References

[1] Y. Bouznit and A. Henni, "Characterization of Sb doped SnO2 films prepared by spray technique and their application to photocurrent generation," *Mater Chem Phys*, vol. 233, no. April, pp. 242–248, 2019, doi: 10.1016/j.matchemphys.2019.05.072.

[2] P. Sivakumar, H. S. Akkera, T. Ranjeth Kumar Reddy, G. Srinivas Reddy, N. Kambhala, and N. Nanda Kumar Reddy, "Influence of Ga doping on structural, optical and electrical properties of transparent conducting SnO2 thin films," *Optik (Stuttg)*, vol. 226, Jan. 2021, doi: 10.1016/j.ijleo.2020.165859.

[3] R. Guo *et al.*, "Significant performance enhancement of all-inorganic CsPbBr3 perovskite solar cells enabled by Nb-doped SnO2 as effective electron transport layer," *Energy and Environmental Materials*, vol. 4, no. 4, pp. 671–680, Oct. 2021, doi: 10.1002/eem2.12213.

[4] X. Zhou *et al.*, "Solution-processed Cu-doped SnO2 as an effective electron transporting layer for High-Performance planar perovskite solar cells," *Appl Surf Sci*, vol. 584, May 2022, doi: 10.1016/j.apsusc.2022.152651.

[5] J. Zhang *et al.*, "Increasing the oxygen vacancy density on the TiO2 surface by La-doping for dye-sensitized solar cells," *Journal of Physical Chemistry C*, vol. 114, no. 43, pp. 18396–18400, Nov. 2010, doi: 10.1021/jp106648c.

[6] H. Wang *et al.*, "W-doped TiO2 as electron transport layer for high performance solution-processed perovskite solar cells," *Appl Surf Sci*, vol. 563, Oct. 2021, doi: 10.1016/j.apsusc.2021.150298.

[7] P. Sivakumar, H. S. Akkera, T. Ranjeth Kumar Reddy, G. Srinivas Reddy, N. Kambhala, and N. Nanda Kumar Reddy, "Influence of Ga doping on structural, optical and electrical properties of transparent conducting SnO2 thin films," *Optik (Stuttg)*, vol. 226, Jan. 2021, doi: 10.1016/j.ijleo.2020.165859.

[8] G. Turgut and E. Sönmez, "Synthesis and characterization of Mo doped SnO2 thin films with spray pyrolysis," *Superlattices Microstruct*, vol. 69, pp. 175–186, 2014, doi: 10.1016/j.spmi.2014.02.009.

[9] H. Choi *et al.*, “Cesium-doped methylammonium lead iodide perovskite light absorber for hybrid solar cells,” *Nano Energy*, vol. 7, pp. 80–85, 2014, doi: 10.1016/j.nanoen.2014.04.017.

[10] H. Chen *et al.*, “Enhanced Performance of Planar Perovskite Solar Cells Using Low-Temperature Solution-Processed Al-Doped SnO2 as Electron Transport Layers,” *Nanoscale Res Lett*, vol. 12, no. 1, Dec. 2017, doi: 10.1186/s11671-017-1992-1.

[11] N. Zhou, Q. Cheng, L. Li, and H. Zhou, “Doping effects in SnO2 transport material for high performance planar perovskite solar cells,” *J Phys D Appl Phys*, vol. 51, no. 39, Aug. 2018, doi: 10.1088/1361-6463/aad685.

[12] C. Bhoomanee, P. Ruankhama, S. Choopun, A. Prathan, and D. Wongratanaphisan, “Effect of Al-doped zno for electron transporting layer in planar perovskite solar cells,” in *Materials Today: Proceedings*, Elsevier Ltd, 2019, pp. 1259–1267. doi: 10.1016/j.matpr.2019.06.014.

[13] P. Sakthivel *et al.*, “Efficient and stable planar perovskite solar cells using co-doped tin oxide as the electron transport layer,” *J Power Sources*, vol. 471, Sep. 2020, doi: 10.1016/j.jpowsour.2020.228443.

[14] H. V. Quy and C. W. Bark, “Ni-Doped SnO2as an Electron Transport Layer by a Low-Temperature Process in Planar Perovskite Solar Cells,” *ACS Omega*, vol. 7, no. 26, pp. 22256–22262, Jul. 2022, doi: 10.1021/acsomega.2c00965.

[15] S. Zhuiykov, *Nanostructured Semiconductor Oxides for the Next Generation of Electronics and Functional Devices*. Elsevier Inc., 2013. doi: 10.1533/9781782422242.

[16] J. Bahadur, A. H. Ghahremani, B. Martin, T. Druffel, M. K. Sunkara, and K. Pal, “Solution processed Mo doped SnO2 as an effective ETL in the fabrication of low temperature planer perovskite solar cell under ambient conditions,” *Org Electron*, vol. 67, pp. 159–167, Apr. 2019, doi: 10.1016/J.ORGEL.2019.01.027.

[17] S. Sajid, S. Alzahmi, I. Ben Salem, and I. M. Obaidat, “Perovskite-Surface-Confined Grain Growth for High-Performance Perovskite Solar Cells,” *Nanomaterials*, vol. 12, no. 19, p. 3352, Oct. 2022, doi: 10.3390/NANO12193352/S1.

[18] Y. J. Kim *et al.*, "Enhanced Light Harvesting in Photovoltaic Devices Using an Edge-Located One-Dimensional Grating Polydimethylsiloxane Membrane," *ACS Appl Mater Interfaces*, vol. 11, no. 39, pp. 36020–36026, Oct. 2019, doi: 10.1021/ACSAMI.9B09377/SUPPL_FILE/AM9B09377_SI_001.PDF.

[19] X. Zhou *et al.*, "Solution-processed Cu-doped SnO2 as an effective electron transporting layer for High-Performance planar perovskite solar cells," *Appl Surf Sci*, vol. 584, p. 152651, May 2022, doi: 10.1016/J.APSUSC.2022.152651.

[20] S. Miyake, S. Fujihara, and T. Kimura, "Characteristics of oriented LaNiO3 thin films fabricated by the sol–gel method," *J Eur Ceram Soc*, vol. 21, no. 10–11, pp. 1525–1528, Jan. 2001, doi: 10.1016/S0955-2219(01)00056-5.

[21] Z. Arshad *et al.*, "Magnesium doped TiO2 as an efficient electron transport layer in perovskite solar cells," *Case Studies in Thermal Engineering*, vol. 26, p. 101101, Aug. 2021, doi: 10.1016/J.CSITE.2021.101101.

[22] Q. Dong, Y. Shi, C. Zhang, Y. Wu, and L. Wang, "Energetically favored formation of SnO2 nanocrystals as electron transfer layer in perovskite solar cells with high efficiency exceeding 19%," *Nano Energy*, vol. 40, pp. 336–344, Oct. 2017, doi: 10.1016/J.NANOEN.2017.08.041.

[23] Y. Qiang *et al.*, "Enhanced performance of carbon-based perovskite solar cells with a Li+-doped SnO2 electron transport layer and Al2O3 scaffold layer," *Solar Energy*, vol. 201, pp. 523–529, May 2020, doi: 10.1016/j.solener.2020.03.046.

[24] C. Bi, Q. Wang, Y. Shao, Y. Yuan, Z. Xiao, and J. Huang, "Non-wetting surface-driven high-aspect-ratio crystalline grain growth for efficient hybrid perovskite solar cells," *Nat Commun*, vol. 6, Jul. 2015, doi: 10.1038/ncomms8747.

[25] H. Mao *et al.*, "Surface grain boundary passivation via mixed antisolvent and PC 61 BM assistant for stable perovskite solar cells," *Journal of Materials Science: Materials in Electronics*, vol. 30, no. 4, pp. 3511–3520, Feb. 2019, doi: 10.1007/S10854-018-00628-8/TABLES/3.

[26] H. Mao *et al.*, “Surface grain boundary passivation via mixed antisolvent and PC 61 BM assistant for stable perovskite solar cells,” *Journal of Materials Science: Materials in Electronics*, vol. 30, no. 4, pp. 3511–3520, Feb. 2019, doi: 10.1007/S10854-018-00628-8.

[27] N. Ali *et al.*, “Enhanced stability in cesium assisted hybrid 2D/3D-perovskite thin films and solar cells prepared in ambient humidity,” *Solar Energy*, vol. 189, pp. 325–332, Sep. 2019, doi: 10.1016/J.SOLENER.2019.07.081.

[28] Q. Liu *et al.*, “Effect of tantalum doping on SnO2 electron transport layer via low temperature process for perovskite solar cells,” *Appl Phys Lett*, vol. 115, no. 14, Sep. 2019, doi: 10.1063/1.5118679.

Chapter 06
Conclusions and Recommendations

This chapter presents an array of results obtained from the comprehensive research conducted, as well as discussing potential future directions for further exploration of the subject matter.

6.1 Conclusions

In conclusion, both pristine and La:SnO_2 ETL were successfully synthesized through a low-temperature refluxing process making them suitable for planar perovskite solar cells. In addition, the compatibility of these ETLs was examined with a mixed-cation mixed-halide perovskite layer that was developed under ambient conditions. The optimal ETL exhibited an increased transparency of 84.2% with 4% La-doped SnO_2, surpassing that of pristine SnO_2. The characterization and analysis of La-doped SnO_2 revealed enhanced conductivity and decreased bandwidth which led to suppressed charge recombination, accelerated charge transfer, and electron excitation at the perovskite/ETL interface, as evidenced by photoluminescence quenching. Additionally, 4% La-doped SnO_2 had a positive impact on film quality and perovskite crystal growth in ambient, resulting in larger grains and an improved light absorption profile, which is beneficial for device performance and current densities. Contact angle measurements indicated the hydrophobic nature of $Cs_{0.1}MA_{0.9}Pb(I_{0.9}Br_{0.1})_3$ films deposited on 4% La-doped ETL, which hampered moisture ingress and could contribute to the long-term stability of PSCs under ambient conditions. This study demonstrates the potential of 4% La-doped SnO_2 as electron transport materials for improved quality of the subsequent mixed-cation mixed-halide perovskite layer for highly efficient and stable planar perovskite solar cells.

6.2 Future Recommendations

The following future recommendations aim to address key areas of interest and explore new opportunities in the development and application of lanthanum-doped tin oxide electron transport layers for perovskite solar cells.

1. Optimization of Lanthanum Concentration: Further research should investigate the optimal concentration of lanthanum doping in tin oxide electron transport layers for enhanced performance and stability of perovskite solar cells.
2. Alternative Doping Elements: Exploration of other doping elements in tin oxide electron transport layers may lead to the discovery of superior materials with improved properties for perovskite solar cells.
3. Device Stability: Long-term stability studies of lanthanum-doped tin oxide electron transport layers in perovskite solar cells should be conducted to assess their performance under various environmental conditions.
4. Scalability: Research on scalable fabrication methods for lanthanum-doped tin oxide electron transport layers in perovskite solar cells will enable commercialization and widespread adoption of the technology.
5. Interface Engineering: Investigate the impact of interface engineering between the lanthanum-doped tin oxide electron transport layer and the perovskite layer to improve charge transport and reduce recombination losses.
6. Tandem Solar Cells: Study the integration of lanthanum-doped tin oxide electron transport layers in tandem solar cells with different bandgap materials, such as silicon, to achieve higher overall efficiencies.

Summary

This chapter summarizes the results obtained from the comprehensive research on lanthanum-doped tin oxide electron transport layers (ETLs) for perovskite solar cells, highlighting the enhanced properties and performance achieved through doping. The optimal ETL showed increased transparency, improved conductivity, and better energy level alignment, leading to suppressed charge recombination and accelerated charge transfer. Additionally, the hydrophobic nature of perovskite films on La-doped ETLs contributed to potential long-term stability.

Future recommendations include optimizing lanthanum concentration, exploring alternative doping elements, studying device stability, researching scalable fabrication methods, examining interface engineering, and integrating La-doped tin oxide ETLs into tandem solar cells. These recommendations aim to further advance the development and application of lanthanum-doped tin oxide electron transport layers in perovskite solar cells.

Appendix-A: Journal Article

Effect of lanthanum doped SnO_2 on the performance of mixed-cation mixed-halide perovskite for planar PSCs

Sana Mehmood[a,], *Nadia Shahzad[a], Saad Nadeem[a], Muhammad Salik Qureshi[a], Abdul Sattar[b], Naseem Iqbal[a], Rabia Liaquat[a], Muhammad Imran Shahzad[c]

[a]*U.S.-Pakistan Centre for Advanced Studies in Energy (USPCAS-E), National University of Sciences & Technology (NUST), H-12 Sector (44000) Islamabad, Pakistan*
[b]*Energy Materiaux Telecommunications Research Center, Institut National de la Recherche Scientifique (INRS-EMT), Quebec, Canada*
[c]*Nanosciences and Technology Department (NS&TD), National Centre for Physics (NCP), 44000 Islamabad, Pakistan*

*Corresponding Author's Email: nadia@uspcase.nust.edu.pk

ABSTRACT

Perovskite solar cells (PSCs) have attracted significant attention due to their higher efficiencies and lower fabrication costs. But for the better performance of PSCs, a high-quality electron transport layer (ETL) is crucial. Various ETLs have been employed and among them Tin (IV) oxide (SnO_2) has emerged as a promising candidate for electron selective layer in PSCs due to its superior optical and electrical characteristics. However, there is still improvement needed in terms of poor surface morphology and conductivities of SnO_2. When SnO_2 is used in conjunction with absorber layer in ambient conditions, stability, and charge carrier recombinations at SnO_2/perovskite interface remains a serious challenge as well. This study presents the doping of lanthanum (La III), a rare earth element, into SnO_2 ETLs to improve the quality and performance of the perovskite layer deposited on top of ETL in ambient condition. With the optimized 4% La (III) doping, SnO_2 ETLs become more crystalline with lower parasitic light absorption and surface morphology improves significantly. The improvement in morphology due to doping facilitates larger crystal growth of perovskite in ambient environment. Moreover, Photoluminescence reveals that with optimized level of doping, interfacial charge recombinations are significantly mitigated ensuring smooth injection of electrons into ETL because of superior perovskite film quality. The mixed-cation mixed-halide perovskite film deposited on 4% La-doped ETL show better resistance towards moisture ingress and will substantially contribute to develop long-life of planar PSCs.

Keywords: electron transport layer, mixed-cation, mixed-halide, perovskite, ambient fabrication, elemental doping

Appendix-B: Journal Article

Solution-Processed Zn_2SnO_4 / ZTO Electron Transport Layers for Planar Perovskite Solar Cells

Saad Nadeem[a], *Nadia Shahzad[a], Sana Mehmood[a], Muhammad Salik Qureshi[a], Abdul Sattar[b], Rabia Liaquat[a], Sehar Shakir[a], Muhammad Imran Shahzad[c]

[a]*U.S.-Pakistan Centre for Advanced Studies in Energy (USPCAS-E), National University of Sciences & Technology (NUST), H-12 Sector (44000) Islamabad, Pakistan*
[b]*Energy Materiaux Telecommunications Research Center, Institut National de la Recherche Scientifique (INRS-EMT), Quebec, Canada*
[c]*Nanosciences and Technology Department (NS&TD), National Centre for Physics (NCP), 44000 Islamabad, Pakistan*

*Corresponding Author's Email: nadia@uspcase.nust.edu.pk

ABSTRACT

Perovskite solar cells (PSCs) have acquired popularity owing to their high efficiency, ease of fabrication, and affordability. In this context, the development of electron transport layers (ETLs) for highly efficient planar photovoltaic devices has received considerable attention. This study investigates the potential of zinc-tin based ternary metal oxide ETLs for application in planar PSCs. Solution-processed methods were used to fabricate crystalline zinc stannate (Zn_2SnO_4), amorphous zinc-tin oxide (ZTO), and Zn_2SnO_4 / ZTO based bilayer films, and their structural, morphological, and optoelectronic properties were studied. XRD and scanning electron microscopy images showed enhanced crystallite size and better surface morphology of perovskite films deposited on bilayer ETL. These ETLs exhibited uniform coverage and high transmittance of up to 90% in the visible spectrum with a band gap range from 4.14 eV for ZTO ETL to 4.29 eV for bilayer ETL. Whereas Photoluminescence studies and Hall effect measurements revealed superior charge extraction, an improved charge carrier mobility (21.84 $cm^2V^{-1}s^{-1}$) and enhanced n-type conductivity in the bilayer ETL. Moreover, contact angle analysis of perovskite layer deposited on bilayer ETL showed increased resistance to moisture erosion (52.20°) which is particularly significant given the detrimental effects moisture can have on the performance of PSCs.

Keywords: ternary metal oxides, electron transport layer, bilayer, ambient fabrication, perovskite solar cells

Appendix-C: Journal Article

Comparative study of Ruthenium complexes and organic sensitizer in ZnO based Dye-sensitized solar cell

Muniba Ayub[a], Ahad Hussain Javed[a], *Nadia Shahzad[a], Zuhair S. Khan[a], Sehar Shakir[a], Faroha Liaquat[b], Ghulam Shabir[b], Faisal Abbas[a], Sana Mehmood[a], Muhammad Imran Shahzad[c]

[a]*U.S.-Pakistan Centre for Advanced Studies in Energy (USPCAS-E), National University of Sciences & Technology (NUST), H-12 Sector (44000) Islamabad, Pakistan*
[b]*Department of Chemistry, Quaid-i-Azam University Islamabad 45320, Pakistan*
[c]*Nanosciences and Technology Department (NS&TD), National Centre for Physics (NCP), 44000 Islamabad, Pakistan*

*Corresponding Author's Email: nadia@uspcase.nust.edu.pk

ABSTRACT

Ruthenium dyes are a well-known player in the field of DSSCs due to their structure and presence of a novel metal. Their properties and complexes are studied for almost three decades. Although these sensitizers show better performances, their high cost makes these devices less economical. Organic dyes have recently been explored as an alternative to ruthenium-based dyes due to their easy and low-cost synthesis. This is a comparative study between Ruthenium and organic dyes which analysis dicyanoisophorone and Rhodanine organic dyes with ruthenium complexes. The Ruthenium complex named SZD-3 has shown efficiency of 1.208%. High recombination rate at interfaces of photoanode- dye molecule and photoanode- electrolyte molecule degrades the device performance consequently decreasing open-circuit voltages and short circuit current of the device. ZnO metal oxide structure instability in the presence of Ru-dyes is also a player in the lower output of the devices. While organic sensitizers SMA-06 and PT4N are 10-11% efficient as compared to SZD-3.

Keywords: Sensitizers, Ruthenium Complexes, isophorone sensitizer, Rhodanine Sensitizer, DSSC